International Technical Committee

Chairman:
Pacejka H.B., The Netherlands

Members:
Abe M., Kanagawa Inst. of Techn., Japan
Allen R. W., Systems Techn. Inc., U.S.A.
Ammon D., DaimlerChrysler, Germany
Duvernier M., Michelin, France
Eichberger A., Intec, Germany
Ferrarotti G., MSC, Italy
Fujioka T., Univ. of Tokyo, Japan
Gim G., Hankook, S-Korea
Gipser M., FH Esslingen, Germany
Guan D., Tsinghua University, P.R. China
Guo K., Jilin University, P.R. China
Jansen, S. T. H., TNO, The Netherlands
Koettgen V., LMS, Germany
Lutz A., Robert Bosch AG, Germany
Mancosu F., Pirelli, Italy
Morgat F.-X., Peugeot Citroen, France
Mundl R., Continental AG, Germany
Oertel Ch., FH Brandenburg, Germany
Preschany G., Porsche, Germany
Riepl A., MAGNA STEYR Fahrzeugtechnik, Austria
Sharp R.S., Imperial College London, U.K.
Troùlis M., Ford, Germany
Van Oosten J., MSC, The Netherlands
Wille H.-Ch., VW, Germany

Special thanks to the sponsors of TMVDA04 (in alphabetical order):

BA-CA, BOSCH, Continental AG, DaimlerChrysler, Delft-Tyre (TNO),
Ford Motor Company, Hankook Tires, Intec GmbH, LMS Int., Magna Steyr, Michelin,
MSC.Software, Porsche, PSA Peugeot Citroen, Vienna Convention Bureau

Vehicle System Dynamics
Vol. 43, Supplement, 2005, 3–17

Taylor & Francis
Taylor & Francis Group

3158

Spin: camber and turning

HANS B. PACEJKA*

Delft University of Technology, TNO Automotive, Steenoven 1, PO Box 756, 5700 AT Helmond, The Netherlands

The paper clarifies some important issues connected with wheel slip due to spin. The spin velocity is defined as the component of the rotational velocity of a rolling body normal to the contacting surface. For a tyre we distinguish two possible components of spin: camber and turning. Different from a homogeneous rolling body, the tyre with its peculiar structure may give quantitatively different responses to each of these components. When comparing the steady-state responses with side-slip and with pure turn slip (path curvature) of some analytical tyre models, it turns out that the aligning torque stiffness is equal to the turn-slip side-force stiffness. This reciprocity may be explained by energy considerations. A tyre model featuring spin-induced side-slip loses this reciprocity. This seems to be verified by tyre side-slip and turn-slip tests. Experimental methods and results are discussed. Some peculiar features and the importance of spin in vehicle dynamics are discussed and demonstrated in several applications of the short-wavelength intermediate-frequency tyre (SWIFT) model.

Keywords: Tyres; Camber; Turning; Path curvature; Tyre model; Vehicle dynamics

1. Introduction

Besides the well-known and commonly used slip quantities called the lateral slip (slip angle) and longitudinal slip (slip ratio) we have a third slip input quantity: the spin. The total spin is made up of two possible components: turn slip and camber. The difference in the responses to turn slip and camber that occurs in particular with belted car tyres is discussed. The reciprocity property that appears to occur in linear analytical physical models of the tyre when comparing the side-slip and turn-slip forces and moment coefficients is addressed and the fact that this is not supported by experimental observations is explained. The importance of having available a simulation model of the tyre that features both turn slip and camber as input quantities is illustrated through shimmy and parking applications. Camber is, of course, important for motorcycle cornering manoeuvres. Cars and trucks may suffer from the wandering phenomenon when moving over rutted roads. Here, the lack of sufficient camber stiffness plays an important role. When traversing three-dimensional obstacles such as oblique cleats the tyre is subjected to effective height and camber variations of the road. The non-lagging response part and the assessment of the effective road input and the computed and measured dynamic tyre responses are briefly discussed.

*Email: hbpacejka@hotmail.com

Vehicle System Dynamics
ISSN 0042-3114 print/ISSN 1744-5159 online
http://www.tandf.co.uk/journals
DOI: 10.1080/00423110500140013

2. Camber and turning

Figure 1 illustrates the condition of combined camber and turning while the slip angle remains zero. The camber angle is denoted with γ, the yaw angle with ψ and the path radius with R. The spin slip φ is defined as the ratio of the normal component of the rotational velocity ω and the forward speed V. We have, for the free rolling wheel (no braking or driving),

$$\varphi = -\frac{1}{V}\omega_z = -\frac{1}{V}(\dot{\psi} - \Omega \sin\gamma) = -\frac{1}{R} + \frac{1}{r_e}\sin\gamma. \qquad (1)$$

The spin may be seen as the difference of two curvatures: one of the path of the contact centre and the other of the vertical projection of the peripheral line of the undeformed tilted tyre (here, a circle with radius equal to the effective rolling radius). Because of the flattening of the tyre while being loaded, the belt is distorted and the curvature of the peripheral line may be reduced considerably when loaded on a smooth surface that is assumed to be frictionless. This is in particular the case when the tyre possesses a belt that is approximately cylindrical in shape. The outer surface of the tilted belt is not parallel to the road surface before being loaded. The resulting distortion after loading on the frictionless surface (figure 2) causes a reduction in the curvature due to the large lateral bending stiffness of the belt. When friction is restored and the cambered wheel is rolled forwards along a straight line, the tread elements which are attached to the belt and adhere to the ground are now laterally deflected, thereby making the contact line straight as well. For a motorcycle tyre with a curved belt and for a steel railway wheel the surfaces are already parallel before loading. The distortion will therefore be minimal and the curvature of the peripheral line when loaded on the $\mu = 0$ surface will be considerably larger than that of the car tyre. This may explain the observed relatively small camber stiffness of the car and truck tyre. At the same time, it explains the large difference between the camber and turn slip stiffness of these tyres (if the former is converted to spin stiffness).

For this reason, a camber reduction factor ε_γ has been introduced. The total spin may now be defined as

$$\varphi = -\frac{1}{V}[\dot{\psi} - (1 - \varepsilon_\gamma)\Omega \sin\gamma]. \qquad (2)$$

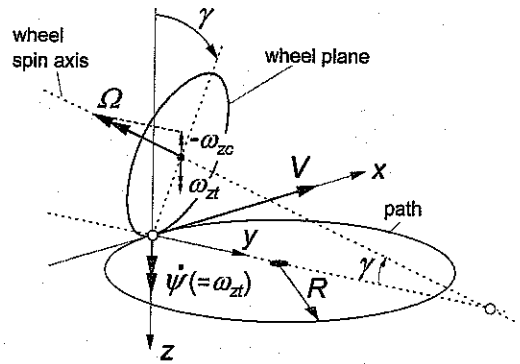

Figure 1. Path curvature (pure turn slip) and camber.

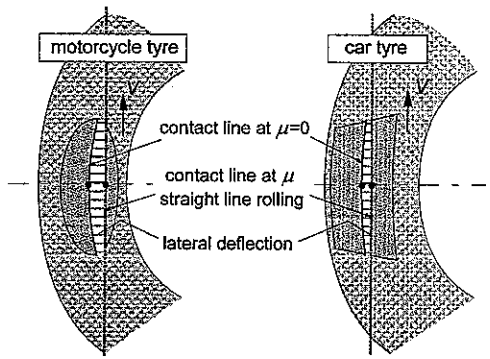

Figure 2. Contact line without and with friction.

Experiments show that the reduction factor can reach values of 50% or more. Later, in section 4, where experimental results are discussed in connection with model analysis, the actual values obtained for a car tyre will be given (see equation (14)).

3. Experiments

Usually, steady-state camber and turn slip measurements are carried out on road or flat track surfaces and on turntable or swing-arm facilities respectively (figure 3). A notable early

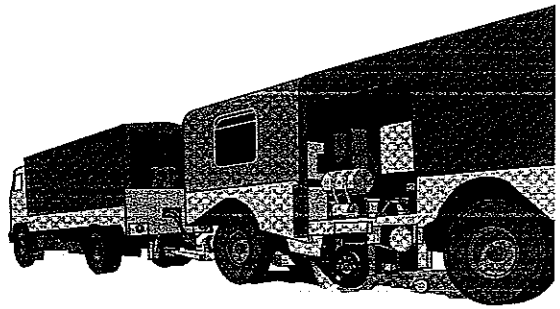

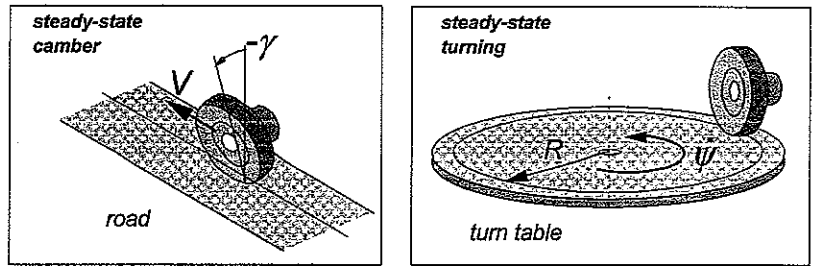

Figure 3. Measurement of steady-state camber and turn-slip response with a test trailer.

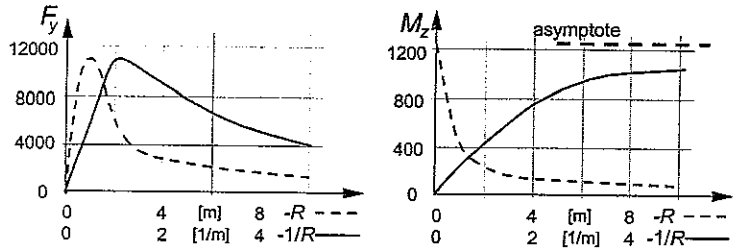

Figure 4. Test results from trailer circular tests for a truck tyre at 20 000 N load [1].

measurement was made by Freudenstein [1]. He used a test trailer that was dragged around in circles. An example of his test results is presented in figure 4. For turn-slip measurements, the available maximum path radius often proves to be too small to assess turn slip stiffness values. These quantities represent the slope of the force or moment characteristics in the origin of the diagrams plotted versus path curvature $-1/R = \varphi$ (with $\alpha \equiv 0$). An alternative method is the derivation of the response to a step change in path curvature from a step change in yaw angle (while the slip angle remains zero) by integration. Figures 5 and 6 clarify the procedure for the test being conducted on a flat plank installation. As illustrated in the lower right diagram of figure 5, the unloaded tyre is first set at a (small) yaw angle, then the tyre is loaded against the still not moving plank and the wheel is turned back so that the wheel centre plane is in line with the plank direction of motion; finally the plank is brought in motion at a low velocity. As depicted in figure 6, at the start, the aligning torque shows a large value because of the antisymmetric distortion of the tyre; the side force is zero. While the wheel rolls, the moment decreases, changes sign and ultimately reduces to zero. The side force starts to build up, reaches a maximum and decays to zero.

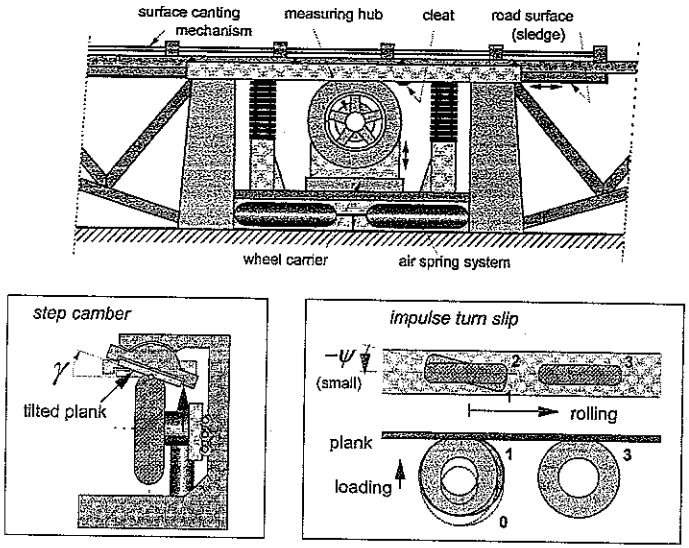

Figure 5. Measurement of step and impulse responses to camber and turning on a flat plank.

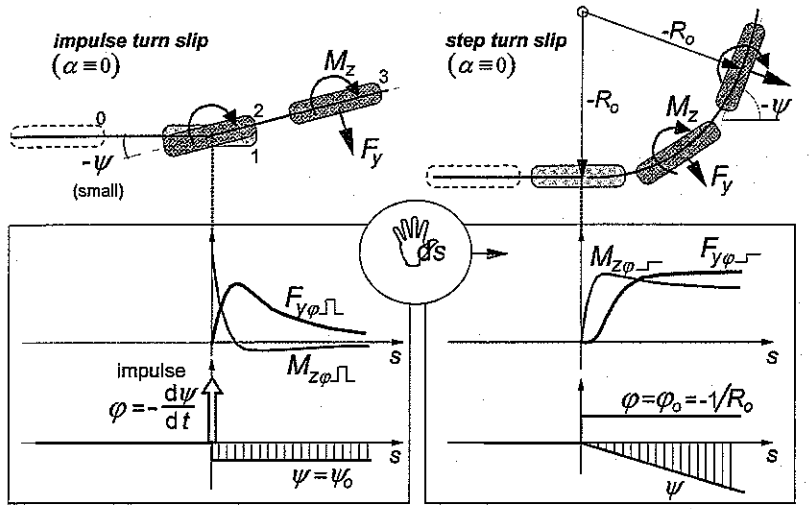

Figure 6. Deriving the step turn-slip response from the impulse turn-slip response.

Integration of these responses leads to the responses to a step change in path curvature as shown on the right-hand side of the figure. Here, the force starts slowly in its development towards the steady-state level. The moment starts at a finite slope, reaches a maximum and approaches its ultimate level. The estimated levels of the horizontal asymptotes provide the steady-state turn slip responses. The integral that is used in the conversion is

$$F_{y\varphi,\text{step}} = -\frac{\varphi_0}{\psi_0} \int F_{y\varphi,\text{pulse}}\, \mathrm{d}s. \tag{3}$$

Step responses to the slip angle and camber angle of the slip quantities are obtained on the flat plank machine in a straightforward manner. For the response to the slip angle, the tyre is put at a yaw angle before it is loaded against the surface, after which the plank is moved. A step change in camber angle test requires a special provision that enables the wheel plane to rotate with respect to the road about the line of intersection of the wheel plane and the road surface. In figure 5, the lower left-hand diagram depicts the principle of the configuration where the road is rotated about that line. The rotation starts when the tyre is already loaded. The position of the wheel axle is held fixed, which causes the load to increase a little. After the desired camber angle is reached, the plank is moved. For more accurate test results, one should first perform a measurement at zero angle with, at the start, the wheel angular position of revolution being the same as in the actual test. The zero-angle test results are then subtracted from the actual test results, which will eliminate variations due to tyre non-uniformities from the final result. These test combinations may then be repeated and averaged for a number of different initial angles of revolution of the wheel.

In figure 7 the step response curves assessed through measurements have been depicted. The levels of step inputs have been kept small to remain approximately in the linear range. The initial yaw angle for the impulse turn slip experiment was $-0.5° = -1/115$ rad which after integration leads, according to equation (3), to a response to a step change in radius of curvature equal to -115 m or $\varphi = 1/115\,\text{m}^{-1}$. The estimated steady-state values can be obtained from the asymptotes of (fitted) curves; then the various slip stiffnesses can be found

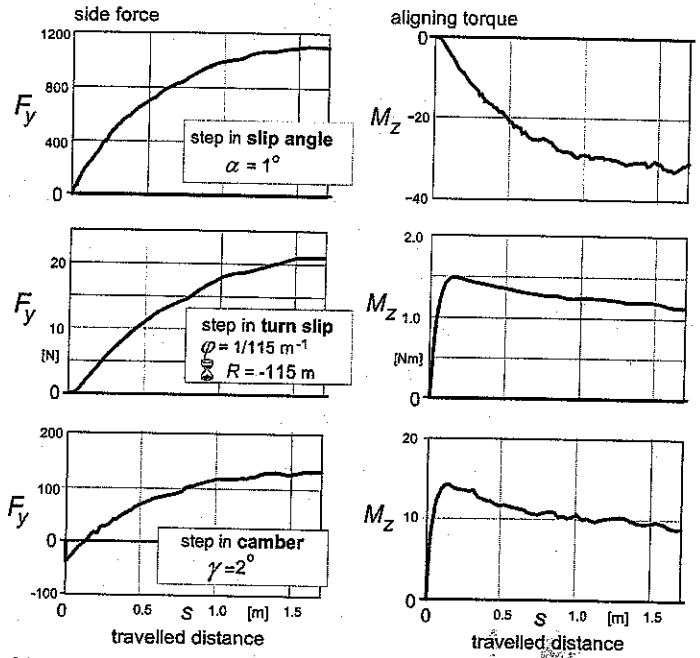

Figure 7. Measured step responses of the side force and the aligning torque to the slip angle, turn slip (path curvature) and wheel camber at a wheel load of 4000 N. (From [1]).

from these estimated steady-state values. The curves in figure 7 show some peculiar features. First of all we have the first-order exponential behaviour of the side-force response to the slip angle, which is well approximated by a first-order differential equation with the relaxation length as the parameter. The moment response deviates a little from this behaviour near the start of the response curve. For a highly loaded aircraft tyre this slow start appears to be much more pronounced. It is striking that the force response to turn slip shows an almost identical behaviour. The moment response to turn slip shows a steep initial slope and a pronounced peak. It is seen that the responses to camber change are very similar to those to turn slip. A remarkable exception is the initial side force that arises as a result of the camber change before the tyre has started to roll. Obviously, it is the asymmetrical deformation of the carcass that produces this side force. Later, we shall discuss this so-called non-lagging part in greater detail. The steady-state values will be used later to interpret analytical results.

4. Mathematical models

A large number of different types of tyre model are available to calculate force and moment responses to wheel input motions. These models range from simple one-dimensional brush models to advanced and complex discrete models based on the physical structure of the tyre. Relatively simple models may be restricted to linear (possibly transient) analyses or to steady-state calculations that may then cover the whole nonlinear and combined-slip range. Semiempirical models are based on formulae that may give accurate representation

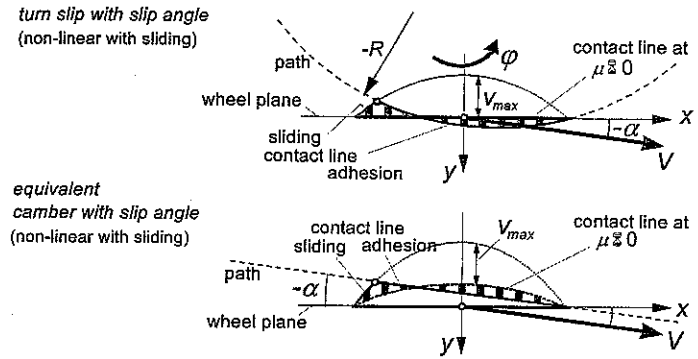

Figure 8. The one-dimensional brush model subjected to side-slip and turn slip or camber.

of measured data. 'Magic formula' descriptions are available for the steady-state forces and moment as a response to the three input slip quantities: longitudinal, lateral and spin slip (camber plus turn slip) and their combinations. First-order nonlinear differential equations are added to cover transient contact phenomena, and second-order equations may be used to deal with the dynamics of the belt. An obvious further advantage of semiempirical models such as the short-wavelength intermediate-frequency tyre (SWIFT) model is the ease of handling in terms of adapting operational parameters such as cornering stiffness, relaxation lengths, vertical stiffness and natural belt frequencies while leaving other properties untouched. The reader should refer to the book by Pacejka [3], the dissertation by Schmeitz [4] and the papers by Besselink *et al.* [5] and Jansen *et al.* [6] presented at the conference and published in this volume for more information on some of these and subsequent models.

In figure 8 the deflected one-dimensional brush model is depicted, which is subjected to a combination of side-slip and turn slip. The lower diagram refers to the equivalent case of combined side-slip and camber. For transient phenomena the stretched-string-based model is more suitable albeit that entering the nonlinear range poses an almost insurmountable difficulty.

Figure 9 shows the development of the string deformation after step changes in side-slip and turn slip. The initial development of the lateral deformation which is uniform in the case of side-slip and angular in the case of turning explains the slow start of the moment and the side-force generation in the respective cases.

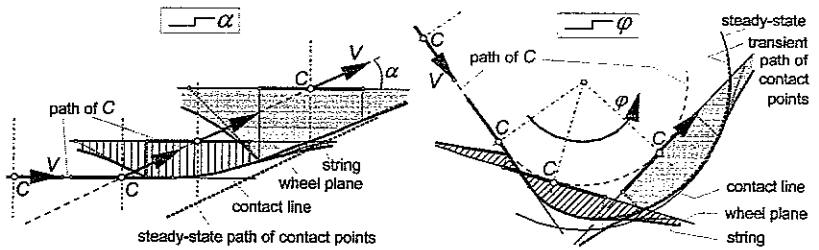

Figure 9. Transient response of the deformation of the stretched-string model to step changes in side-slip and turn slip.

The predicted force and moment responses are very similar to the measured values in figure 7 except for the moment response to turn slip. The ultimate shape of the deformed string is symmetric in the case of turning, which causes the moment to vanish. We need to expand the model and to make it two dimensional, that is to add the finite width of the contact patch. This is accomplished by adding tread elements attached to a number of parallel strings. These elements may be allowed to deflect only in the longitudinal direction. This considerably limits the complexity of this analytical linear model. In figure 10, the two-dimensional model and the resulting response curves have been depicted. The moment response is subdivided into the moment M_z' due to lateral string deformation and the moment M_z^* due to longitudinal deflection caused by the tread width. The shape of the measured response curve is now predicted satisfactorily. It is noted, however, that the contribution of the turn-slip-induced side-slip, to be introduced later, results in a better approximation of the measured curve as well.

To deal with the observed phenomena in a semiempirical model a set of first-order differential equations may be used. The parameters (relaxation lengths) are made load and slip magnitude dependent. SWIFT features in total seven equations: one for κ', two for α' and t (pneumatic trail) and four for φ'. The principal differential equation for the transient turn slip (similar to those for longitudinal slip and lateral slip) is

$$\sigma_\varphi \dot{\varphi}' + V\varphi' = -\dot{\psi}. \tag{4}$$

The structure of the equations allows the use of the equation even at vanishing speed V. Then, the equation reduces to an integral of the yaw rate, which corresponds to a stiffness equation. At speeds approaching zero, the performance of the moment in parking manoeuvres is improved by using, instead, the integral given by van der Jagt [7] for the deflection angle β:

$$\beta = -\int \left(1 - p\frac{|M_z|}{M_{z\infty}}\right)^c \dot{\psi}\, dt. \tag{5}$$

This then should be multiplied by the torsional stiffness of the standing tyre. The coefficient $p = 0$ if $\beta\dot{\psi} > 0$; otherwise $p = 1$. The exponent c may be taken to be equal to 2. The maximum moment occurs at full turn sliding and is denoted by $M_{z\infty}$. As can be seen from the formula, the increase in the deflection angle is decreased when the moment becomes closer to its ultimate maximum. For the actual more complex modelling in SWIFT, see [3]. Later, an application regarding parking manoeuvring will be demonstrated.

The observed reciprocity in the moment response to side-slip and the force response to turn slip is typically demonstrated in the linear steady-state equations. We have for the side force

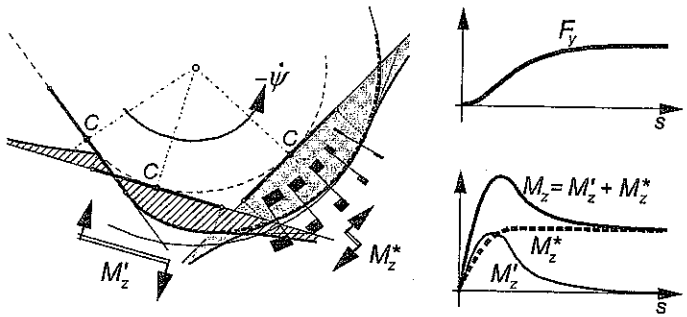

Figure 10. String–brush two-dimensional model for linear transient analysis with resulting step responses.

and the aligning moment

$$F_y = C_{F\alpha}\alpha + C_{F\varphi}\varphi, \tag{6}$$

$$M_z = -C_{M\alpha}\alpha + C_{M\varphi}\varphi, \tag{7}$$

with all slip stiffness coefficients taken as positive quantities. For the analytical brush and string models (possibly extended with laterally deflecting tread elements) it turns out that

$$C_{F\varphi} = C_{M\alpha}. \tag{8}$$

This type of reciprocity with equal but opposite coefficients is known to occur also in dynamic systems, that is in gyroscopic terms. The explanation of this phenomenon may be given by considering the energy flow in the system. For this, the bond graph that corresponds to the equations (6) and (7) may be helpful. Figure 11 shows the bond graph on the left-hand side. As indicated, the power that flows into the system equals the product of the pair of covariables: $P_F = -V_y F_y$ and $P_M = -\dot{\psi} M_z$. Through the 1-junction power $P_{F\varphi} = -V_y F_{y\varphi}$ is diverted towards the gyrator while the remaining power $P_{F\alpha} = -V_y F_{y\alpha}$ is fed to the resistor where that part of the power is dissipated and the side-slip force $F_{y\alpha}$ is produced by multiplying the flow $-V_y$ by the resistor parameter $C_{F\alpha}/V$. In the gyrator, the flow variable $-V_y$ is transformed into the effort variable $-M_{z\alpha}$ through multiplication by the gyrator factor $C_{M\alpha}/V$. In the lower part of the graph the power P_M joins the power that comes from the gyrator. This power $-P_{M\alpha}$ turns out to be equal to the power $P_{F\varphi}$ that originated from the side force due to turn slip. In the lower 1-junction the power $-P_{M\alpha}$ is added to P_M. As a result, the power that is dissipated in the lower resistor is equal to just $P_{M\varphi} = -\dot{\psi} M_{z\varphi}$; that is, it is only associated with turn slip. At steady state, the moment due to turn slip is only due to longitudinal deflections, which leads to the equality $M_{z\varphi} = M_z^*$. As a consequence, we observe that the power $P_{F\varphi} = -V_y F_{y\varphi}$ is converted into $-P_{M\alpha} = \dot{\psi} M_{z\alpha}$, which is then fed back into the system. Consequently, this part of the power that is passed through the gyrator is being conserved, which probably forms the background of the occurrence of the opposite reciprocity. It can be shown that the energy, which is connected with the lateral force and is lost in the rear end of the contact patch, is related to the side force only because of side-slip. The lateral deformation due to turn slip is symmetric and additional sliding does not take place. The energy loss connected with turn slip is due to the longitudinal deflections which abruptly drop to zero at the trailing edge, just like the loss in lateral potential energy at side-slip.

It would be interesting to see whether the same phenomenon is found to occur with the actual tyre. This seems not to be the case. From the estimated heights of the asymptotes of the step function responses presented in figure 7 the following set of slip stiffnesses have been derived: $C_{F\alpha} = 66\,000\,\mathrm{N\,rad^{-1}}$, $C_{M\alpha} = 1900\,\mathrm{N\,m\,rad^{-1}}$, $C_{F\varphi} = 2600\,\mathrm{N\,m}$, $C_{M\varphi} = 120\,\mathrm{N\,m^2}$, $C_{F\gamma} = 4000\,\mathrm{N\,rad^{-1}}$ and $C_{M\gamma} = 230\,\mathrm{N\,m\,rad^{-1}}$. This result shows a considerably larger $C_{F\varphi}$ than

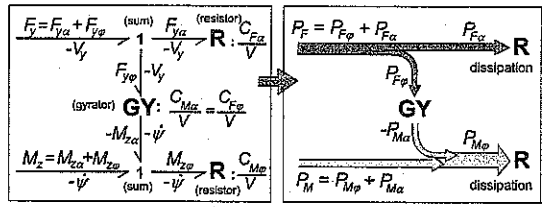

Figure 11. The bond graph representing the relations given by equations (6) and (7), and the connected power flow diagram.

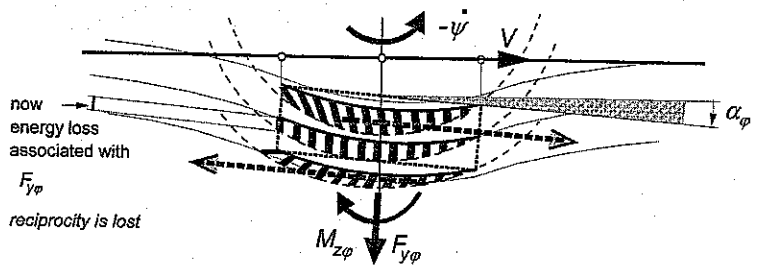

Figure 12. The extended model showing the turn-slip-induced slip angle.

$C_{M\alpha}$. An extended model that takes into account the torsion of the lower part of the belt through the action of the moment M_z^* due to the tread width is capable of eliminating this discrepancy. Figure 12 depicts the extended model that now shows the internal slip angle α_φ caused by the turn-slip moment. Here we see that the lateral deflections at the trailing edge do not vanish, indicating that some power loss is associated with the side force due to turning. As the side force is now slightly pointing to the rear, the dissipated power is compensated by the forward motion of the wheel axle. A bond graph that represents the new system does show that additional connections with the forward power source brings about the loss of reciprocity. The force and moment turn-slip stiffnesses for the extended model can be derived to become

$$C_{F\varphi} = C_{M\alpha} + \frac{C_{F\alpha} C_M^*}{c_\psi}, \tag{9}$$

$$C_{M\varphi} = C_{M\varphi}^* - \frac{C_{M\alpha} C_{M\varphi}^*}{c_\psi}, \tag{10}$$

from which we find the slip stiffness only attributed to longitudinal deflections:

$$C_{M\varphi}^* = \frac{C_{M\varphi}}{1 - C_{M\alpha}/c_\psi}. \tag{11}$$

Equations (9) and (10) indicate that through the induced side-slip the turn-slip stiffness for the side force is increased while the stiffness for the moment is decreased. The first finding is in agreement with experimental evidence as indicated above. From the experimentally obtained slip stiffnesses listed above, the associated torsional stiffness of the lower part of the belt may be derived using the above equations:

$$c_\psi = C_{M\alpha} + \frac{C_{M\varphi} C_{F\alpha}}{C_{F\varphi} - C_{M\alpha}} = 13\,300\,\mathrm{N\,m\,rad^{-1}}. \tag{12}$$

As expected, the value for the torsional stiffness c_ψ is much larger than the experimentally assessed torsional stiffness of the standing tyre including the flexible tread elements: $C_{M\psi} \approx 4000\,\mathrm{N\,m\,rad^{-1}}$. With equation (11) the value for the turn-slip stiffness due to the tread width becomes

$$C_{M\varphi}^* = 140\,\mathrm{N\,m^2}, \tag{13}$$

which, obviously, is larger than the total turn-slip stiffness $C_{M\varphi}$ owing to the counteraction of $C_{M\alpha}$ in equation (10).

From the experimental data listed above with $C_{F\varphi} = 2600\,\mathrm{N\,m}$, $C_{M\varphi} = 120\,\mathrm{N\,m^2}$, $C_{F\gamma} = 4000\,\mathrm{N\,rad^{-1}}$, $C_{M\gamma} = 230\,\mathrm{N\,m\,rad^{-1}}$ and the effective rolling radius $r_e = 0.3\,\mathrm{m}$, the camber reduction factor ε_γ introduced in equation (2) can be calculated. We have the formula

$$1 - \varepsilon_\gamma = r_e \frac{C_\gamma}{C_\varphi}. \tag{14}$$

Using the ratio of the force slip stiffnesses or of the moment slip stiffnesses may lead to different results. We obtain for the force response a camber reduction factor $\varepsilon_\gamma = 0.54$ and for the moment 0.43. As generally the force response to camber is of greater importance than the moment response, we may decide to employ a value closer to that associated with the force.

5. The non-lagging part

As has already been indicated in connection with the step response of the side force to camber change as plotted in the lower left diagram of figure 7, an initial value may already arise because of the asymmetric deformation of the tyre before the tyre starts to roll. The initial value that is generated in the process of loading and applying camber depends on the way that the final configuration is achieved. In figure 13, three independent ways of approach have been considered. After rolling has started, the force develops and the steady-state value is approached. The signs of the initial forces and their magnitudes differ for the three cases and will depend on the magnitude of the camber angle and the normal load. Inclusion of the non-lagging part in simulations, and therefore of the relatively fast response at quick changes in load and camber that might occur on rough roads, may be accomplished by computing the associated lateral tyre deformation. For this, one may employ the differential equation for the transient slip angle with, on the right-hand side, the side-slip velocity which is now a combination of the lateral velocity of the contact centre C and of an additional slip point S_y attached on the wheel radius pointing to the contact centre at a distance r_s (figure 14). The introduction of the additional slip point is obviously necessary to cover the cases R and C

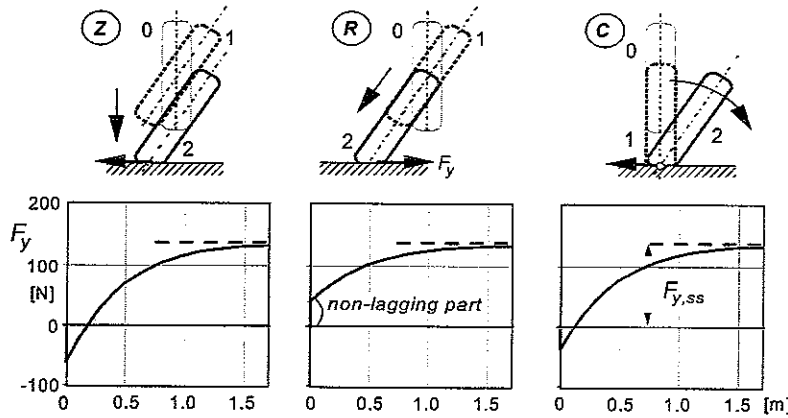

Figure 13. The three principal cases of the response to the changes in loading and camber before and after rolling (camber angle, 2°; vertical load, 4000 N).

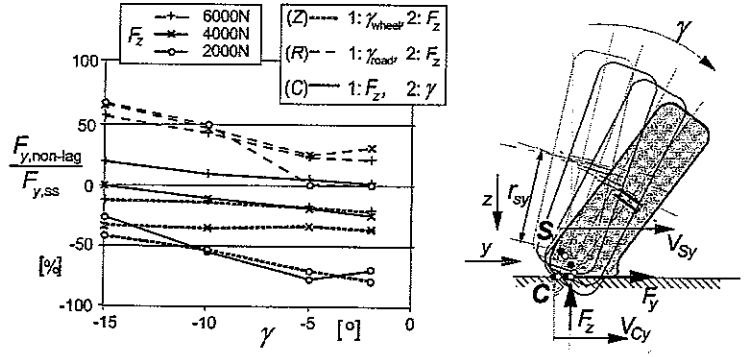

Figure 14. Non-lagging parts (left) [2] and introduction of the second slip point S_y (right).

where the contact centre C does not move laterally. The differential equation is

$$\sigma_\alpha \dot{\alpha}' + V\alpha' = -V_y = -(1-\varepsilon)V_{Cy} - \varepsilon V_{Sy}. \tag{15}$$

If the forward speed V vanishes, the equation takes the form of an integral from which the deflection follows and with $\sigma_\alpha = C_{F\alpha}/C_{Fy}$ the static side force is obtained. Both r_s and ε are functions of the load and camber angle aiming at reproducing the data in figure 14 (left-hand diagram). For the ensuing response at rolling, equation (15) continues to operate. Obviously, the two slip velocity components represent the velocities of the slip points with respect to the local road surface plane. On three-dimensional uneven surfaces, this plane changes in orientation, thereby causing relative camber changes.

6. Applications

We shall first address examples that demonstrate the importance of turn-slip properties in vehicle dynamics. It is always the moment that makes turn slip an important factor in some applications. With camber, it appears that the camber thrust (force) is the more important output.

Two items will be discussed briefly, that is wheel shimmy and parking. Wheel shimmy is the well-known, self-excited and sometimes dangerous oscillation that may occur with the aircraft landing gear and the front wheels of trucks. The pneumatic tyre, often in combination with the lateral compliance of the wheel suspension, can be the cause of this type of instability. When oscillating the rolling wheel about its vertical axis the aligning torque $-M_z'$ shows a phase lag with respect to the imposed (small) yaw angle ψ. In the model, this is caused by the differential equation (15). For straight-ahead motion of the wheel centre, the side-slip velocity $-V_y$ is proportional to ψ. Hence, α' will lag behind ψ. At low frequencies we may put $M_z' = -C_{M\alpha}\alpha'$. The lag is responsible for the destabilizing energy flow into the system that ultimately comes from the forward motion of the vehicle. The turn-slip moment $-M_z^*$, however, provides damping since it shows a phase lead of approximately 90° with respect to ψ because at low frequencies this moment is proportional to $-\varphi$, that is to $\dot{\psi}/V$. In figure 15, areas of instability are shown where shimmy will develop without external excitation. Unstable ranges of speed V have been plotted versus the mechanical trail e. The area of instability diminishes and ultimately vanishes at increasing turn-slip stiffness $C_{M\varphi}$.

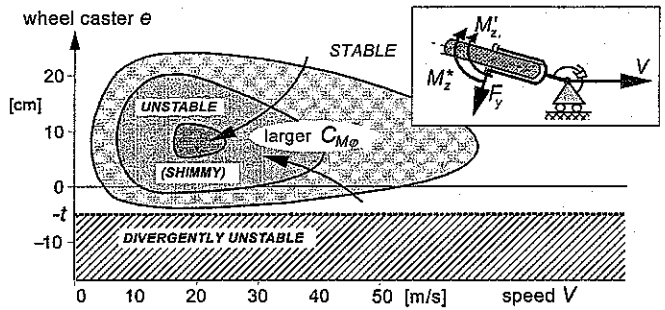

Figure 15. Area of shimmy instability which shrinks at larger turn-slip stiffnesses [3].

Manoeuvring at a low speed while turning the steering wheel gives rise to relatively large steering torques. This effect is largely due to the turn-slip moment $M_{z\varphi}$. In the SWIFT algorithm, four first-order differential equations are used (equation (4) is one of them) to cover the relatively complex short-wavelength contact patch properties connected with turn slip. 'Magic formula' extensions generate the output force and moment. To describe the parking moment variations at zero speed or a very low speed of travel better, the algorithm gradually changes to the full use of the integral (5). Figure 16 (left-hand diagram) compares test and computed results showing the variation in the moment about the central vertical wheel axis while the axle is swivelled about the same axis. The initial part of the curve can be improved by adapting the exponent c in equation (5). In the right-hand diagram the simulation is extended to the phase where the axle starts to move forwards while the steering input remains unchanged. The steering axis is connected to a quarter-vehicle body and it is observed that the side force is beginning to develop as the speed increases. A small lateral vibration appears to show up at low speeds, which is connected with the car mass moving side ways on the compliant tyre.

Camber produces a side force when the wheel is tilted with respect to the road surface. For motorcycles this is the main source of the side thrust needed for cornering. For cars and trucks, camber is often an input that can better be avoided. Special cars may employ camber to minimize wear and to maximize side-force generation (at side-slip). Local road camber caused by rutted roads may give rise to the so-called wandering effect that is due to insufficient camber stiffness such as generally occurs with radial tyres. The wheel does not climb up or stay neutral

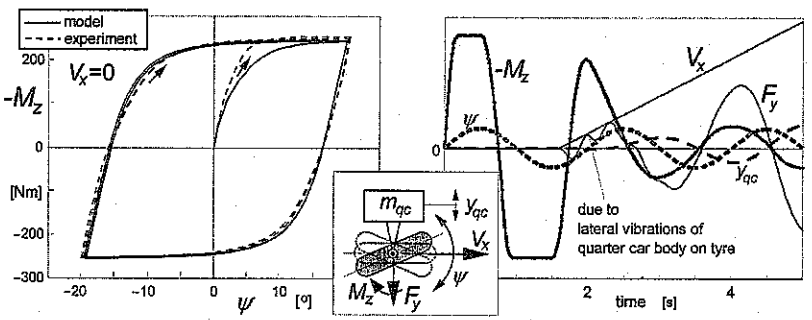

Figure 16. The non-rolling tyre loaded on a flat plank and steered back and forth (left) and with a quarter-car mass that begins to move forwards (simulation) (right).

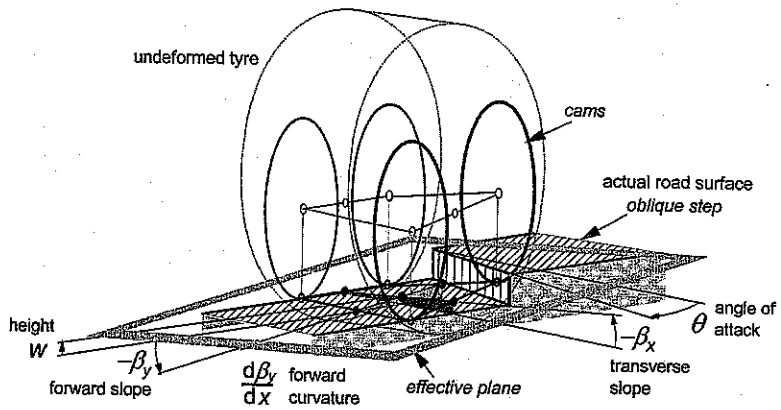

Figure 17. Double-track tandem-cam road feeler (effective road inputs; oblique step).

but tends to move to the lowest path in the rut. On three-dimensional uneven road surfaces the local road plane shows variations in height, in forward slope and in transverse slope. The latter gives rise to tyre camber variations that must be taken into account to simulate the force variation felt by the wheel properly. Since the tyre has a finite contact length and width, geometric filtering occurs and the so-called enveloping power of the tyre plays an important role. To model rolling over uneven roads and traversing obstacles, the concept of the effective road plane has been introduced. With such an effective input, a tyre model with a single-point road contact can be employed. In addition to the three effective quantities mentioned, a fourth input is used: the effective forward road curvature that is used to vary the effective rolling radius properly. To assess the effective input variables, a road feeler is developed that consists of a set of cams arranged along the edges of the rectangular contact zone. The cams can move

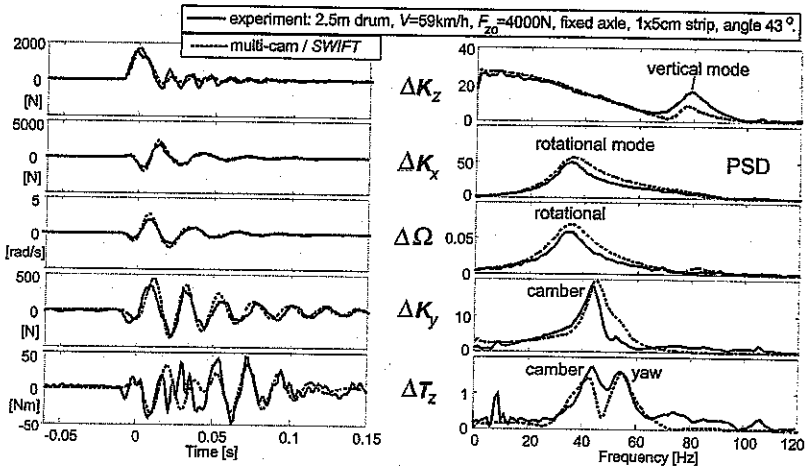

Figure 18. Vertical, longitudinal and lateral forces and aligning axle moment as measured and simulated: PSD, power spectral density.

vertically, guided by the wheel axle, and touch the actual road surface. The average height and slopes of the surface that contains the lowest points of the cams provide the effective inputs. Usually, a pair of four cams is needed. For more detailed and especially oblique obstacles, more cams may be needed to scan the surface more accurately (figure 17). Figure 18 gives an example of dynamic measurement and simulation results. The wheel axle is fixed and the tyre rolls over an oblique cleat. Time traces and power spectral densities have been presented (see [4] for more details).

References

[1] Freudenstein, G., 1962, Luftreifen bei Schräg- and Kurvenlauf. *Deutsche Kraftfahrtforschung und Straßenverkehrstechnik*, **152**.
[2] Higuchi, A., 1997, Transient response of tyres at large wheel slip and camber. Dissertation, Technische Universiteit Delft, Delft, The Netherlands.
[3] Pacejka, H.B., 2002, *Tyre and Vehicle Dynamics* (Oxford: Butterworth–Heinemann).
[4] Schmeitz, A.J.C., 2004, A semi-empirical three-dimensional model of the pneumatic tyre rolling over arbitrarily uneven road surfaces. Dissertation, Technische Universiteit Delft, Delft, The Netherlands.
[5] Besselink, I.J.M., *et al.*, 2005, *Vehicle System Dynamics, Supplement*, **43**, 63–75.
[6] Jansen, S.T.H., Verhoeff, L., Cremers, R., Schmeiz, A.J.C. and Besselink, I.J.M., 2005, *Vehicle System Dynamics, Supplement*, **43**, 92–101.
[7] van der Jagt, P., 2000, The road to virtual vehicle prototyping. Dissertation, Technische Universiteit Eindhoven, Eindhoven, The Netherlands.

Vehicle System Dynamics
Vol. 43, Supplement, 2005, 18–29

Taylor & Francis
Taylor & Francis Group

Implementations, applications and limits of tyre models in multibody simulation

ALEX EICHBERGER* and MARCUS SCHITTENHELM

INTEC GmbH, Argelsrieder Feld 13, 82234 Wessling, Germany

The article focuses on the interface between multibody software and tyre models as well as on the applications and limitations of tyre models implemented in multibody codes. Basic principles of multibody simulation will be followed by a classification of the range of applications of multibody codes for vehicle dynamics design and assessment and the corresponding classification of tyre models in multibody simulation. The classification will be made along occurring oscillation amplitudes ranging from very small to large part displacements and along occurring frequencies ranging from quasistatic movements up to the acoustic frequency range. The basic structure of the interfaces between tyre model, road description and multibody model will be revealed and the different call modes of tyre models in multibody codes will be summarized. As examples some industrial applications of tyre models in multibody simulation will be explained. This includes quasistatic tyre model-based simulation scenarios as well as lateral and longitudinal dynamic simulation scenarios in quite a low-frequency range and finally vertical and combined dynamic simulation scenarios in higher-frequency ranges.

Keywords: Multibody simulation; Tyre models; SIMPACK

1. Introduction

Tyre models in multibody programs are used for a huge variety of simulation tasks in vehicle dynamics design. This includes lateral and longitudinal vehicle dynamics in quite a low-frequency range up to vertical vehicle dynamics in a high-frequency range and combinations. Many different proprietary and non-commercial tyre models have been developed in the past and still are under steady development and improvement. The vast number of different tyre models often causes the simulation engineer to be spoilt for choice when choosing a proper model for a certain simulation task. The situation becomes even more complicated when tyre models with road descriptions are interfaced to multibody codes in many different ways.

To find out the best tyre model suitable for a certain simulation task a classification of the range of applications of multibody codes for vehicle dynamics design and assessment is necessary. The classification can be made along occurring oscillation amplitudes ranging from very small to large part displacements and along occurring frequencies ranging from quasistatic movements up to the acoustic frequency range. In a second step, the existing tyre models have to be fitted into the application classification scheme.

*Corresponding author. Email: alex.eichberger@simpack.de

Vehicle System Dynamics
ISSN 0042-3114 print/ISSN 1744-5159 online © 2005 Taylor & Francis
http://www.tandf.co.uk/journals
DOI: 10.1080/00423110500109349

The same tyre model can be interfaced in many different ways to multibody programs. The kinematics given by the multibody code has to be transformed to a proper tyre–road-based coordinate system, and the forces and torques produced by the tyre model have to be transferred back to a vehicle-based system. Additionally, tyre models can be algebraic force elements or may have internal dynamics which can be solved in a cosimulation mode or simultaneously by the solver of the multibody code. Tyre models can be used in many different call modes, which can be for instance static analysis, nonlinear dynamic analysis in the time domain or linear dynamic analysis in the frequency domain. When interfacing tyre models to multibody codes, care has to be taken that the interface and the tyre model support all necessary call modes without the need for changing the multibody model.

Even though a huge range of applications can be addressed by today's tyre models in multibody codes there exist limitations, and basic research still needs to be invested, for example easy tyre model parameter determination process, influence of temperature changes, various road conditions (wet, off road, flexible ground, etc.), and influence of ageing process or abrasion.

2. Basics of multibody codes

Besides linear and nonlinear finite-element analysis, multibody simulation has become an established computer-aided engineering-process in the design of the functional dynamic or static behaviour of complete cars, motorcycles and trucks or subsystems such as chassis, engine and driveline. Multibody simulation is a very efficient method to deliver insight and results on motions, forces, accelerations, frequencies, loads, noise, vibrations, ride comfort, handling performance, stability and many more.

2.1 *Modelling approach*

The modelling approach for multibody models differs from the modelling approach for finite-element models. Figure 1 shows the front-wheel suspension of a cross-country vehicle.

The technical system wheel suspension can be regarded as consisting of bodies including mass and inertia, which are linked together by massless idealized joints and force elements. Which technical part is to be modelled as body or joint or force element is the responsibility of the engineer and depends on the intended simulation task. Figure 2 shows a very simplified multibody representation of the wheel suspension. It consists of four bodies: chassis, suspension arm, wheel carrier and steering rack. The bodies produce the inertia forces. The bodies are linked together by one revolute joint, one universal joint, two connection rods and one prismatic joint. Bodies and joints define the kinematics and the motion degrees of freedom. Applied forces are induced by the force elements: leaf spring, shock absorber, gravity and tyre. Additional multibody elements are the inertial reference frame and sensors that measure positions, velocities and accelerations and excitations.

2.2 *Multibody equations*

The basic principles for setting up the motion equations of multibody systems have been known since Lagrange, Newton, Euler and d'Alembert. Depending on the choice of generalized coordinates and applying the principles of mechanics, one derives the motion equations in one

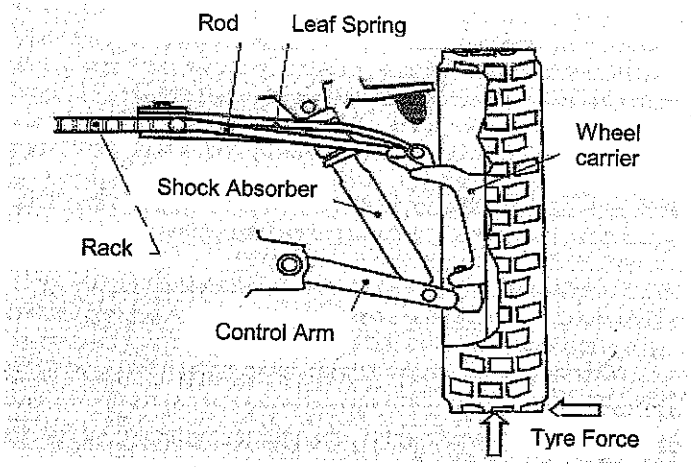

Figure 1. Front-wheel suspension of a cross-country vehicle.

of two forms. Firstly, in state space form for a minimum set of state variables $\boldsymbol{x}$,

$$\begin{aligned} \dot{\boldsymbol{x}}_\mathrm{p} &= \boldsymbol{x}_\mathrm{v}, \\ \mathbf{M}\dot{\boldsymbol{x}}_\mathrm{v} &= \boldsymbol{h}(\boldsymbol{x}_\mathrm{p}, \boldsymbol{x}_\mathrm{v}, t), \end{aligned} \tag{1}$$

where $\boldsymbol{x}_\mathrm{p}$ denotes the state position variables, whereas $\boldsymbol{x}_\mathrm{v}$ contains the state velocity variables. The dot above a symbol means the derivative with respect to time t. $\mathbf{M}$ represents the mass and inertia matrix, and $\boldsymbol{h}$ is the vector of generalized applied forces. In words, equation (1) expresses the mechanical principle that mass times acceleration equals the applied forces.

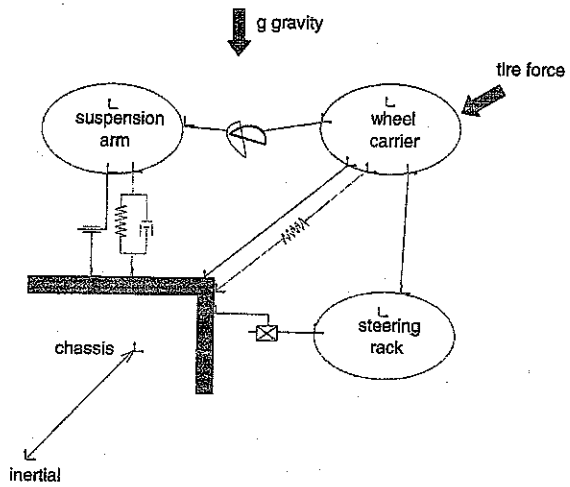

Figure 2. Multibody model of the front-wheel suspension.

The state space form of the motion equations are nonlinear ordinary first-order differential equations. Secondly, in description form for a set of redundant variables $\boldsymbol{z}$,

$$\begin{aligned} \dot{\boldsymbol{z}}_\mathrm{p} &= \boldsymbol{z}_\mathrm{v}, \\ \mathbf{M}\dot{\boldsymbol{z}}_\mathrm{v} - \mathbf{G}^\mathrm{T}\boldsymbol{\lambda} &= \boldsymbol{h}(\boldsymbol{z}_\mathrm{p}, \boldsymbol{z}_\mathrm{v}, t), \\ \boldsymbol{g}(\boldsymbol{z}_\mathrm{p}, t) &= \mathbf{0}, \end{aligned} \tag{2}$$

where $\boldsymbol{z}_\mathrm{p}$ denotes the redundant position variables, whereas $\boldsymbol{z}_\mathrm{v}$ contains the redundant velocity variables. The dot above a symbol means the derivative with respect to time t. Matrix $\mathbf{M}$ represents the mass and inertia matrix, and $\boldsymbol{h}$ is the vector of generalized applied forces. Matrix $\mathbf{G}$ represents the constraint modes of motion and $\boldsymbol{\lambda}$ the constraint forces. Vector $\boldsymbol{g}$ describes the constraint equations on the position level. The descriptor form of the motion equations are nonlinear ordinary first-order differential algebraic equations (DAE).

In both formulations the right-hand side $\boldsymbol{h}$ contains the tyre forces which depend on the vehicle position and velocity. In the case when the tyre model is an element with internal dynamic states, both equation (1) and equation (2) have to be expanded by the following differential equation of the tyre states $\boldsymbol{x}_\mathrm{T}$:

$$\dot{\boldsymbol{x}}_\mathrm{T} = \boldsymbol{f}(\boldsymbol{x}_\mathrm{T}, t). \tag{3}$$

2.3 *Multibody solver modes*

Different numerical solver options can be applied to the motion equations.

Directly solving equations (1)–(3) in the time domain by nonlinear *numerical time integration* yields the motion, the kinematic quantities on position, velocity and acceleration level and the constraint and applied forces (e.g. tyre forces). This solver mode is applied for instance in vehicle-handling performance analysis, for hardware-in-the-loop and software-in-the-loop applications, for ride comfort investigations, for noise vibration and harshness improvement and in load data generation for durability and fatigue analysis.

Linearizing the motion equations, one ends up with the linearized first-order differential equation

$$\dot{\boldsymbol{x}} = \mathbf{A}\boldsymbol{x} + \mathbf{B}\boldsymbol{u}, \tag{4}$$

where $\boldsymbol{x}$ contains the state position and velocity variables of the linearized system. Matrix $\mathbf{A}$ is the constant state space matrix, $\mathbf{B}$ is the system input matrix and $\boldsymbol{u}$ contains the input signals to the system. Equation (4) is the basic equation for a *linear system analysis* in the frequency domain, yielding the natural frequencies, damping, eigenmodes, frequency response functions, linear system response and power spectral density. This solver mode is very central processor unit time efficient even for complex models and in a high-frequency range. This mode is used for oscillation analysis, comfort analysis and acoustics design for vehicles.

Setting the derivatives in equations (1)–(3) equal to zero yields the static or quasistatic representation of the motion equations in the general form

$$\mathbf{0} = \boldsymbol{f}(\boldsymbol{x}, t), \tag{5}$$

where $\boldsymbol{x}$ contains the position and velocity variables of the static or quasistatic system. Nonlinear numerical algebraic solvers such as Newton iteration are applied to equation (5) for *static and quasistatic analysis*. This solver mode is being used in kinematic and compliant kinematic suspension analysis, for computing the static prestress forces and equilibrium positions and static loads.

In order to use one vehicle multibody model for all solver modes, it is essential that the tyre model directly supports the nonlinear time integration mode, the linear frequency mode and the nonlinear static and quasistatic modes.

3. Classification of vehicle dynamics simulation tasks

Multibody models are applied to a huge variety of standard simulation tasks such as handling analysis, suspension analysis, driving comfort, stability and safety and durability load data generation.

Figure 3 gives an overview of the classification in terms of occurring frequencies and amplitudes and reveals the typical borders for multibody simulation.

4. Classification of tyre models

Tyre models can be classified by the physical modelling approach and additionally by use cases. Both approaches are briefly summarized.

Simple tyre models are often a linear or nonlinear spring–damper combination for pure vertical vehicle dynamics. For taking into account lateral and longitudinal tyre forces a linear relation between slip and resulting force is applied. Combined slip is not taken into account. Simple tyre models are used for static and quasistatic vertical and lateral analyses of the vehicle often in combination with virtual test rigs. They are also used for basic handling simulations and are contained in vehicle models for hardware-in-the-loop applications or vehicle control design environments. Because of the linear nature of the slip–force relation the usefulness for quantitative lateral and longitudinal vehicle behaviour is very limited. As there are no belt dynamics included, it can be applied to a very-low-frequency range only. Figure 4 shows the typical application range of simple tyre models.

The so-called *approximation models* are based on a nonlinear mathematical approximation of the tyre forces from measured longitudinal and lateral tyre behaviours. Combined slip

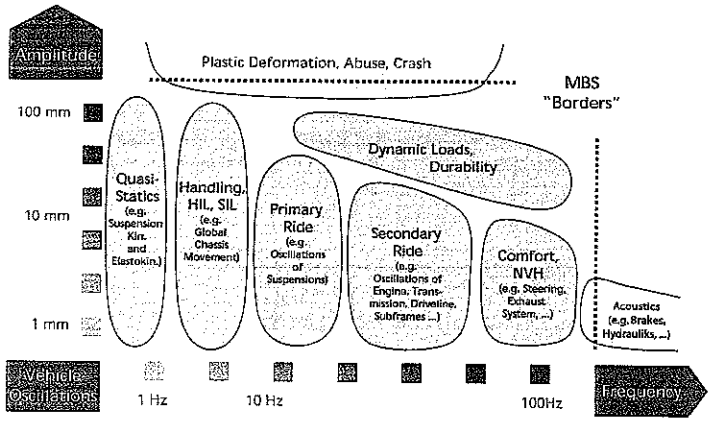

Figure 3. Classification of vehicle dynamics simulation tasks: MBS, multibody system; HIL, hardware in the loop; SIL, software in the loop; NVH, noise vibration harshness.

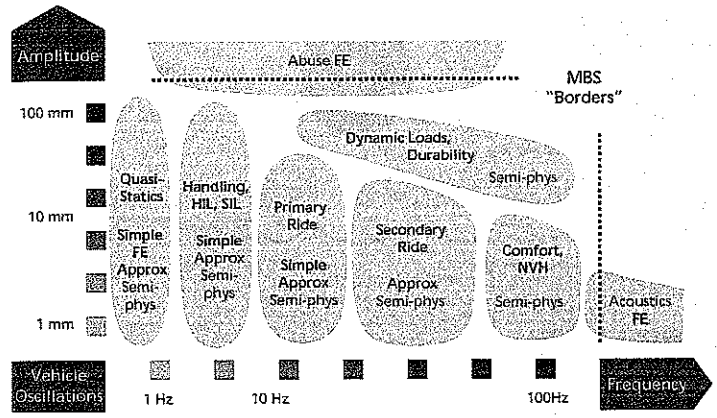

Figure 4. Classification of tyre models by use cases: FE, finite element; MBS, multibody system; HIL, hardware in the loop; SIL, software in the loop; NVH, noise vibration harshness.

can be taken into account. The model can be combined with a linear or nonlinear spring–damper combination for vertical vehicle dynamics. Increasingly the approximation model is combined with a rigid ring that has six degrees of freedom and that is supported by a spring–damper model with respect to the rim. Some approximation models also have a discretizeted belt model. According to figure 4, these tyre models can be found in static and quasistatic simulation tasks, but the main range of application is handling dynamics, as well as primary ride and secondary ride. Limitations to this tyre models are very high frequencies above 60 Hz and the very short wavelength of road unevenness.

Physical or semiphysical models or deformation models describe the kinematics and dynamics of the rubber ribs in the contact patch area in detail. The brush model is a well-known candidate for this kind of tyre model. To derive the parameters of the model no slip–force measurements are necessary as the describing parameters are of a physical and geometrical nature. These models can be also combined with a simple linear or nonlinear spring–damper combination for vertical vehicle dynamics, with the rigid-ring tyre model or with a highly discretizeted belt model. Figure 4 shows that the application range is not limited, but these kinds as of tyre model are mainly used for static and quasistatic applications, secondary ride, comfort and noise vibration harshness simulations and durability load profile generation.

Finite-element tyre models consist of a detailed finite-element structure for the contact patch area, the belt and the gas dynamics. These models allow one to take into account any physical effect of tyre behaviour but the computational effort is high. Finite-element tyre models are being used for highly detailed static applications, for abuse investigations or in a high-frequency range when dealing with noise emission.

5. Interfaces between tyre models and multibody codes

There exist more than 20 different commercial and in-house multibody codes on the market. This huge number is combined with even a higher number of different tyre models (Pacejka MF 87, Pacejka Similarity, HSRI, MF Tyre, MF-MC Tyre and SWIFT Tyre). Taking SIMPACK as an example, the user can choose between six different tyre models which mainly are

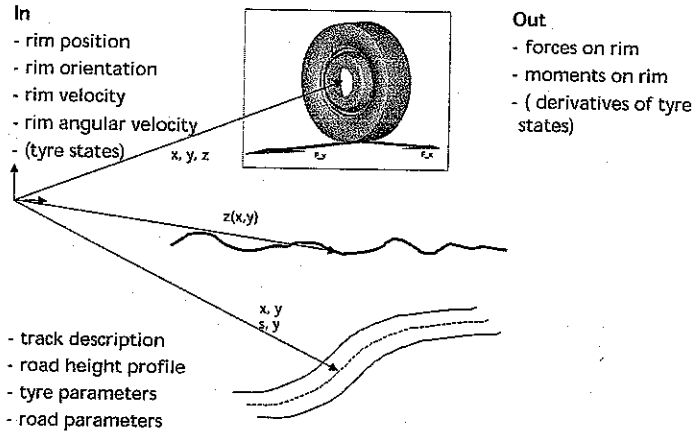

Figure 5. Basic input and output quantities of tyre models in multibody codes.

approximation and deformation models (Pacejka MF 87, Pacejka Similarity, HSRI, MF Tyre, MF-MC Tyre and SWIFT Tyre). Additionally, interfaces to more than ten different approximation and deformation tyre models have been implemented (e.g. TM-Easy, RMOD-K, F-Tire, Brit, IPG-Tyre and Fiala Tyre). All interfaces use a common basis but differ in detail. At first glance, the interface is very straightforward.

On the input side, the tyre and road model needs kinematic information on the rim with respect to the inertia frame. This consists of the three Cartesian position and velocity states, three orientation angles and the angular velocities. In the case when the tyre model has internal dynamic states, these are also input to the model. The tyre and road models are described by the track description, road height profile, road condition parameters and tyre parameters. For each right-hand side call of equations (1) or (2) the tyre model has to provide the forces and moments acting on the rim and in the case of a dynamic model according to equation (3) also the time derivatives of the internal tyre states.

The implementation of the interface is shown in figure 6.

Some tyre models have their own road model or an interface to a road model. In this case, the multibody model transfers the kinematic quantities and the tyre states if necessary with a certain call mode to the tyre model. The tyre model passes the kinematic position information to the road model and receives the road height profile. In the next step the tyre model computes the forces and moments acting on the rim as well as the derivative of the tyre state variables and transfers these quantities to the multibody code for the next time integration step. In order to link different multibody codes easily with different tyre and road models, a standard tyre interface (STI) and a standardized tyre model–road model interface has been agreed upon.

As an alternative the road model has to be addressed by the multibody code. In this case the kinematic position and orientation of each wheel have to be transferred by the multibody code to the road model, which in turn gives back the road height profile which is then passed through to the tyre model. The interface between multibody codes and road models is not standardized.

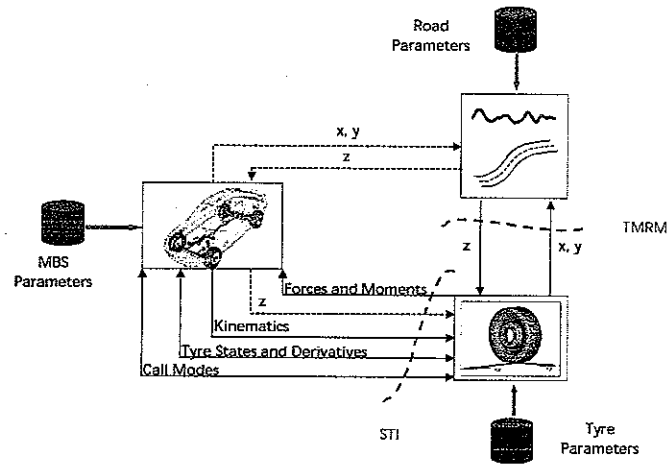

Figure 6. Interfaces between multibody model, tyre model and road model: MBS, multibody system; TMRM, tyre model–road model; STI, standard tyre interface.

Special attention has to be drawn to the different call modes of tyre models. The most important call modes are as follows:

(i) nonlinear continuous-in-time domain;
(ii) nonlinear discrete-in-time domain (cosimulation mode);
(iii) stable real-time mode at a given sample period;
(iv) linear continuous-in-time domain;
(v) eigenmode analysis (mode shapes, natural frequencies and damping);
(vi) linear frequency and system response;
(vii) standstill operation mode, both in the time domain and the frequency domain;
(viii) parking operation mode;
(ix) tyre force characteristics mode;
(x) four-roller test rig mode;
(xi) four-poster stamp test rig mode;
(xii) tyre test rig mode.

The objective is to use the same tyre model and multibody model for all operation modes listed above. This requires enhancements of today's tyre models as well as the enhancements of interfaces on the side of the multibody codes. Accordingly the STI also has to be further expanded.

6. Application examples of tyre models in multibody codes

At present, most of the relevant tyre properties are well understood and can be represented by the tyre models existing today. The range of today's typical applications will be shown by the following examples.

6.1 *Lateral and longitudinal dynamics*

Figure 7 shows a sinusoidal steering manoeuvre at different vehicle speeds. It is a typical manoeuvre for assessing the lateral agility and the lateral acceleration response due to steering input. Besides a detailed model of the suspension compliant kinematics of the multibody model of the car, the static and transient lateral tyre characteristics are crucial for meaningful results. In this case an approximation tyre model has been used.

Figure 8 shows an example of a lane change manoeuvre of a car with caravan at different speeds. One purpose of those simulations is for example to test or design the control code of an electronic stability management system. Again the virtual prototype requires a detailed suspension model together with a realistic approximation of the lateral and longitudinal static and transient tyre behaviour. Owing to braking inputs from the stability system, combined lateral and longitudinal slip has to be taken into account. In this case an approximation tyre model has been used.

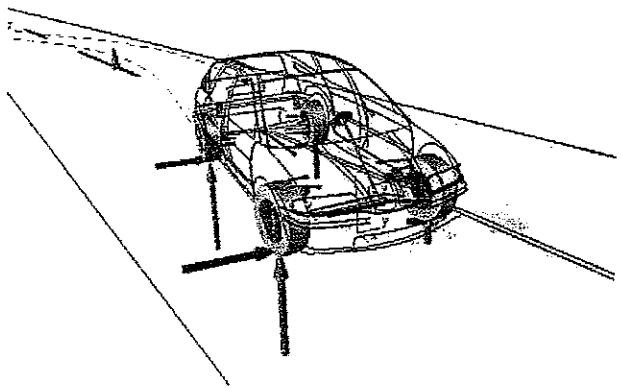

Figure 7. Sinusoidal steering manoeuvre.

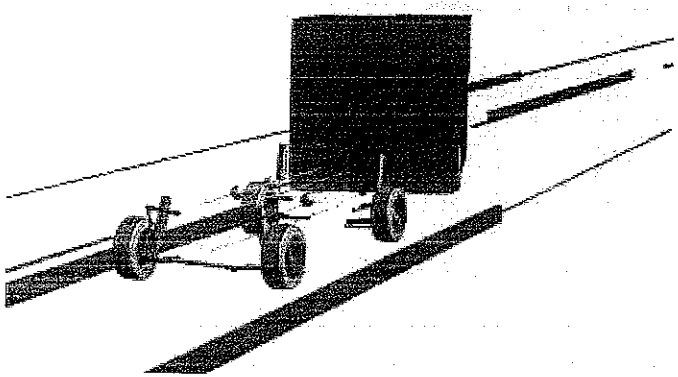

Figure 8. Lane change manoeuvre with trailer.

Figure 9. Lane change manoeuvre in limit conditions.

Figure 9 shows a lane change manoeuvre in limit conditions. Testing the stability at different load conditions of the trailer is investigated with those simulations. Because of simultaneous cornering and braking, a good representation of combined dynamics of lateral and longitudinal forces is a prerequisite for reliable results. Additionally the tyre model must be able to represent the forces and moments due to large camber angles. The simulations have been carried out with an approximation model.

6.2 *Vertical and longitudinal dynamics*

Figure 10 shows a car driving on a poor road surface with short wavelength. The point of interest of this simulation is the vertical dynamics for instance to generate durability load profiles or to assess the ride comfort. The multibody model is highly detailed and includes flexible bodies. The tyre model must be able to represent the high-frequency dynamics of all

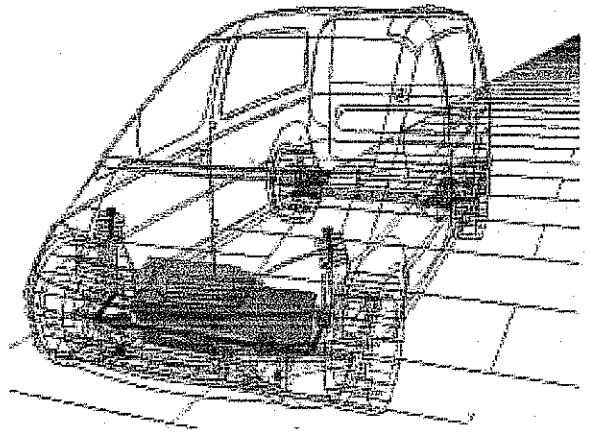

Figure 10. Car on an uneven road.

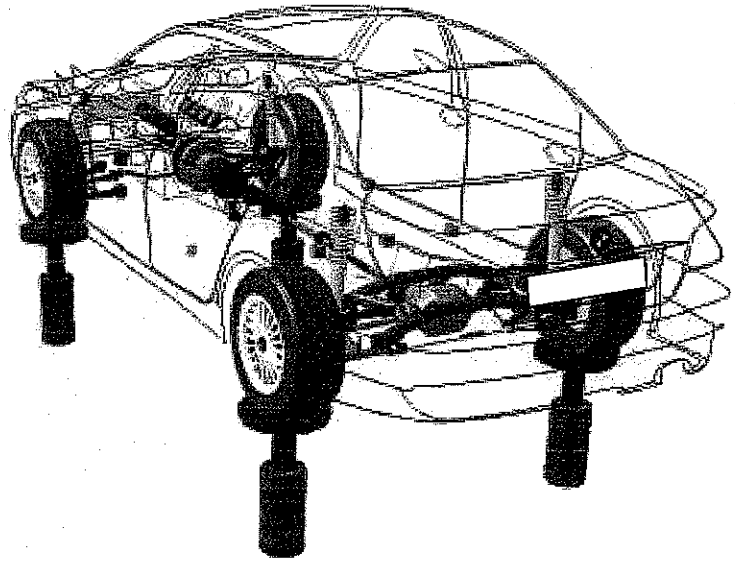

Figure 11. Car on a four-poster stamp rig.

tyre force components. Also the dynamics of the tyre belt vibrations have to be included in the longitudinal direction and also in vertical direction. To produce correct longitudinal forces, a detailed tyre–road contact model is included. For this simulations a semiphysical tyre model has been used.

The last application example is shown in figure 11. The model consists of a detailed suspension model including compliance at the mount points of the suspension parts. Also the flexibility of the subframe is taken into account. All components of the drive train are modelled in detail in order to obtain a good representation of all oscillation effects. The excitation of the posters reaches from low to higher frequencies. The tyre model has to support a standstill operation mode and the dynamics of the tyre belt must be represented as well. For small excitation amplitudes a linearization mode has to be supported. For this simulation an approximation tyre model with an elastic belt has been used.

7. Summary

The article focused on the interface between multibody software and tyre models. Basic and common principles of multibody codes were shown, followed by a summary of different simulation modes for vehicle dynamics simulation. The application range of multibody codes was classified in terms of simulation tasks, frequencies and excitation amplitudes and this classification scheme was transformed to classify also the different tyre models. The principal structure of the interfaces between multibody codes and tyre models was explained together with the need for standardizing and further enhancing the scope of these interfaces in order to support as many different call modes for the same tyre model. Application examples for lateral, longitudinal and vertical vehicle behaviour prove that today the combination of tyre models and multibody codes is well established for standard simulation tasks in vehicle

dynamics simulation. Additionally, specialists are able to generate reliable results even for non-standard simulation tasks where higher frequencies, multipoint contact and/or huge deflection amplitudes occur. A safe and economically reasonable process for obtaining the parameters of the different tyre models and recommendations on how to handle the uncertainty in the tyre measurements which are the basis for the parametrization process are still open issues. Concentrating on few different tyre models which are easy to exchange and which support all operation and call modes would help non-experts greatly to carry out their simulation tasks. The tyre model performance test is a good source of information and will give a good first orientation for selecting a proper tyre model for an individual simulation task.

References

[1] Arnold, A., 2004, Numerische Verfahren in der Mehrkörperdynamik. In: *SIMPACK Academy* (Hirschem: INTEC GmbH).
[2] Eichberger, A., 2002, Generating multibody real-time models for hardware-in-the-loop Applications. In: *Proceeding of the 8th International Symposium on Advanced Vehicle Control*, Hiroshima, Japan, 2002.
[3] Eichberger, A., 1994, Transputer-based multibody system dynamic simulation, Part I: the residual algorithm – a modified inverse dynamic formulation. *Mechanics of Structures and Machines*, **22**, 211–237.
[4] Kortüm, W. and Lugner, P., 1994, *Systemdynamik und Regelung von Fahrzeugen* (Berlin: Springer).
[5] Popp, K. and Schiehlen, W, 1993, *Fahrzeugdynamik* (Stuttgart: Teubner).
[6] Roberson, R.E. and Schwertassek, R., 1988, *Dynamics of Multibody Systems* (Berlin: Springer).
[7] Rulka, W., 1998, Effiziente Simulation der Dynamik mechatronischer Systeme für industrielle Anwendungen. PhD thesis, Technical University of Vienna, Austria.

3.2 *Validity of the cornering force–self-aligning torque system model*

Figure 5 shows the slip-angle dependence of F_y and M_z for tyres A–C, together with the results of the fit to the CF–SAT system model and the transient change in $p(x_1)$. For any tyres, the results of the fit to the CF–SAT system model agree well with the measurements. While the saturated value of $F_y(a)$ at larger slip angles ($a > 10°$) is mainly determined by the load F_z and the sliding friction coefficient μ_d of tread rubber, the value of $F_y(a)$ at more practical handling angles ($a < 5°$) depends on the adhesive friction coefficient μ_s and the deformation stiffnesses of the tyre (*i.e.* C_y, ϵ and G_{mz}). The longitudinal-force torque $M_{zx}(a)$ is fairly large and becomes dominant at larger slip angles. In a previous study which had compared the measured cornering property with the analytical theory [7], it was reported that the theoretical fit of $M_z(a)$ was poorer than that of $F_y(a)$. In the CF–SAT system model, this problem is improved by the introduction of $M_{zx}(a)$, the description of which is too simple.

4. Conclusions

A new analytical tyre model for the CF and SAT is proposed on the basis of the Fiala model. The CF–SAT system model describes the slip-angle dependences of the CF and SAT by forms consistent with a common set of deformation stiffnesses of the tyre casing and the friction coefficients of tread rubber. The system model, which contains both the physical meaning of parameters and the precise description of measured cornering data, might be applicable to tyre designs, vehicle cornering simulations and other purposes. Least-squares fits to the model reveal the adhesive–sliding fraction of the contact patch during cornering.

References

[1] Delft-Tyre, 1996, *MF-Tyre User Manual (Version 5.0). A Design and Analysis Tool for Modelling and Simulation of Tyre Behaviour* (Delft: Delft-Tyre, TNO Automotive).

[2] Pacejka, H.B. and Besselink, I.J.M., 1997, Magic formula tyre model with transient properties. *Vehicle System Dynamics, Supplement*, **27**, 234–249.

[3] Pacejka, H.B., 2002, *Tyre and Vehicle Dynamics* (Oxford: Butterworth–Heinemann).

[4] Fiala, E., 1954, Seitenkräfte am rollenden Luftreifen, *VDI Zeitschrift*, **96**(29).

[5] Kabe, K. and Miyashita, N., 2005, A study of the cornering force by use of analytical tyre model. *Vehicle System Dynamics Supplement*, **43**, 125–134.

[6] Gim, G. and Nikravesh, P.E., 1990, An analytical model of pneumatic tyres for vehicle dynamic simulations, Part 1: pure slips. *International Journal of Vehicle Design*, **11**(6), 589–618.

[7] Sakai, H., 1981, Theoretical and experimental studies on the dynamic properties of tyres, Part 1: review of theories of rubber friction. *International Journal of Vehicle Design*, **2**(1), 78–110.

[8] Miyashita, N., Kawazura, T. and Kabe, K., 2003, Analytical model of μ–S curve using the skewed-parabola. *JSAE Review*, **24**(1), 81–86.

[9] Sakai, H., 1982, *Tyre Mechanics* (in Japanese) (Japan: Grand-Prix Co.).

[10] Sakai, H., 1989, Study on cornering properties of tire and vehicle. *Tire Science and Technology*, **18**(3), 136–169.

Vehicle System Dynamics
Vol. 43, Supplement, 2005, 135–144

Taylor & Francis
Taylor & Francis Group

The rolling resistance of truck tyres under a dynamic vertical load

ARNAUD J. P. MIEGE† and ATANAS A. POPOV*‡

†QinetiQ, Land Vehicle Systems, Cody Technology Park, Building X80, Room 218, Ively Road, Farnborough GU14 0LX, UK
‡School of Mechanical, Materials and Manufacturing Engineering, University of Nottingham, University Park, Nottingham NG7 2RD, UK

The paper deals with tyre modelling to predict the rolling resistance of truck tyres under a dynamic vertical load. A model originating from Pacejka is applied and modified to perform the necessary calculations. The predictions are compared with the available experimental data on rolling resistance under dynamic vertical load given by Popov *et al.* The analysis is extended into a larger frequency range so that other models can be also discussed and compared. Within the frequency range considered and based on the experimental data, Pacejka's model appears to give the best results.

Keywords: Pneumatic tyres; Rolling resistance; Heavy vehicles; Dynamic vertical load; Tyre modelling

1. Introduction

The rolling resistance accounts for approximately one third of the energy consumed by a heavy vehicle engine [1]. Significant economic and environmental improvements can be obtained by reducing fuel consumption and therefore rolling resistance. The loss comes from energy dissipation in both the tyres and the suspension of the vehicle. For a freely rolling tyre under a static vertical load, it can be measured on large rotating drum with a smooth surface [2]. The measured rolling resistance arises from hysteretic losses in the sidewalls and tread band material, which experience a deformation cycle every revolution of the tyre [3]. There is an additional small loss (approximately 10%) due to microslip in the contact patch between tyre and test surface.

Three major mechanisms exist by which the road roughness can produce additional losses [3] (figure 1):

(a) excitation of the vehicle by road roughness, leading to energy dissipation in the suspension dampers and frictional losses due to vibration;

*Corresponding author. Email: Atanas.Popov@Nottingham.ac.uk

Vehicle System Dynamics
ISSN 0042-3114 print/ISSN 1744-5159 online © 2005 Taylor & Francis
http://www.tandf.co.uk/journals
DOI: 10.1080/00423110500140039

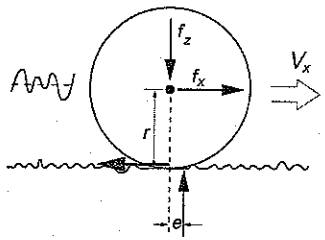

Figure 1. Tyre rolling resistance. From Popov *et al.* [7].

(b) hysteretic losses in the contact patch due to dynamic vertical deflection of the tyres, and additional frictional losses in the contact patch due to microslip;
(c) hysteretic losses in the tyre material due to envelopment of the road roughness by the tyre, which also cause further frictional losses in the contact patch due to microslip.

This energy dissipation results in an asymmetric pressure distribution, which is higher in the forward portion of the contact patch, where the tread elements are forced radially inwards, and lower in the rearward portion of the contact patch, where the tread elements are forced radially outwards [4]. This leads to a forward shift in the centroid of the normal pressure distribution, at a distance e in figure 1, where the horizontal and vertical forces applied at the wheel hub react. A moment balance about an axis through a point on the road surface below the wheel centre yields the following relationship:

$$f_x r - f_z e = 0 \Longrightarrow \frac{f_x}{f_z} = \frac{e}{r}, \tag{1}$$

where V_x is the forward speed of the vehicle, f_x and f_z are the longitudinal and vertical forces respectively acting at the wheel axle†, r is the loaded radius of the tyre and e is the longitudinal shift of the line of action for the vertical contact force. The ratio e/r is by definition the rolling resistance of the tyre.

Schuring [2] wrote an extensive review on the rolling resistance of tyres in steady-state conditions under a constant vertical load. The influence of operation conditions as well as tyre design parameters on rolling resistance were investigated. The findings were mainly of experimental nature although some tyre models (empirical, thermal, viscoelastic and thermo-viscoelastic) were referred to for the prediction of rolling resistance. These models gave conflicting results, highlighting the difficulty in modelling rolling resistance accurately and shedding some doubt over the validity of the predictions by the available theoretical models.

Klingbeil [5] and Klingbeil *et al.* [6] developed a viscoelastic model for rolling resistance calculations where rolling losses were associated with seven deformation mechanisms in the tyre structure. These rolling losses were computed through harmonic analyses of all deformation cycles and the application of a loss tangent factor to the maximum stored strain energy for each spectral component. The results showed that the main contributions to the rolling resistance were from bending of the tread band, compression of the tread and shearing of the sidewalls. Comparison with experimental data showed general good agreement with the predicted trends but there were some discrepancies in the absolute values. Popov *et al.* [3] used this method for truck tyres. However, only the rolling resistance component due to tread compression was considered, which was found to amount to approximately 56% of the measured value of rolling resistance.

†Throughout the paper, f_x and f_z will refer to forces in the time domain, whereas F_x and F_z will refer to forces in the frequency domain.

Although a large volume of research exists on the steady rolling resistance of tyres under a constant vertical load, very few studies have considered the energy dissipation in the tyre and suspension together. Most of the existing literature is concerned with car tyres and few data are available on truck tyres, which have a different design and carry substantially higher loads. Furthermore, no laboratory measurements of truck tyre rolling resistance under a dynamic vertical load have been reported until recently; Popov *et al.* [7] showed that there was no significant effect of dynamic load on mean rolling resistance (due to static vertical load), whether on a smooth drum or in the presence of cleats in the frequency range considered (0–4 Hz).

The work described in this paper aims to apply and extend existing tyre models to predict rolling resistance under dynamic vertical load in the frequency range of interest (0–20 Hz) and to compare the results with the available experimental data from Popov *et al.* [7]. Section 2 presents the relevant experimental results from Popov *et al.* [7] of measured rolling resistance under a dynamic vertical load. The tyre model giving the best correlation to those results is presented in section 3, together with a critical comparison with other models. Finally, conclusions are drawn in section 4.

2. Experimental results

A very brief summary of the experimental results from Popov *et al.* [7] is presented here for the purpose of model validation in section 3. For further details, the reader should refer to [7]. A rolling-drum facility of 3 m diameter at Dunlop Tyres Ltd UK was modified to provide a unique dynamic loading and measurement capability. The sensitivity and accuracy of the longitudinal-force measurement were increased substantially by using a non-rotating six-component load cell from the University of Michigan Transportation Research Institute (UMTRI) [8]. Errors due to the load cell misalignment and rotation (caused by vertical wheel displacement) were corrected using displacement transducers. A hydraulic servo-controlled actuator was used to generate a dynamic vertical load on the wheel, superimposed on the static load provided by the existing pneumatic loading system. Accelerometers were used to correct for the acceleration of the mass outboard of the load cell. The measurements were made for two types of tyre: a conventional drive-axle tyre (385/65R22.5) and a wide-base low-profile tyre (295/80R22.5).

2.1 *Measurement procedure*

The tyres were initially warmed up for 2 h with a vertical load close to the test load. The steady inflation pressure reached at the end of the warm-up period was kept constant during the test by a control system. Changes in the temperature of the tyre were minimized by taking measurements immediately after any change in load. Measurements were made at one inflation pressure (9.4 bar warm for the 385/65R22.5 tyre, and 8.7 bar warm for the 295/80R22.5 tyre), three speeds (10, 40 and 80 km h^{-1}) and four harmonic loading frequencies (0.5, 1, 2 and 4 Hz). The static component of the vertical load was within the range used during the steady-state measurements. The amplitude of the dynamic force component was always 50% of the static vertical force.

After the warm-up procedure, the programme of measurements consisted of the following steps for each combination of tyre, static force and speed.

(i) The longitudinal force was measured for the static force alone.
(ii) A harmonic dynamic vertical force was superimposed on to the static vertical force with amplitude 50% of the static value, and the corresponding average longitudinal force was measured for each of the forcing frequencies.

(iii) The dynamic load was then applied quasistatically, in discrete levels, and the longitudinal force was measured at each level.
(iv) The 4 Hz dynamic load was then reapplied and a longitudinal-force measurement taken.

2.2 *Rolling resistance under a dynamic vertical load*

Figure 2 presents the results obtained under a dynamic vertical load for the 385/65R22.5 tyre at 9.4 bar and 40 km h^{-1}, based on data collected through the whole loading programme, with an initial vertical load close to 35 kN. There are two measurements at 4 Hz obtained right at the beginning and the end of the experimental programme; they are in good agreement with each other, which proves the repeatability of the measurements. The best-fit line, which was obtained using the least-squares-error approximation through all data points in figure 2, has a slope close to zero. This indicates little effect of dynamic loading on overall rolling resistance.

It can therefore be concluded that there is little discernible effect of the dynamic vertical load on the mean rolling resistance across a wide range of frequencies. However, this cannot be extrapolated to frequencies much higher than, say, 6 Hz owing to limitations with the experimental set-up.

3. Tyre modelling

Three tyre models [4, 9, 10] were applied and modified to predict the rolling resistance under a dynamic vertical load [11]. These models were selected over others because of their relative ease of implementation and evaluation of model parameters, as well as their ability to model longitudinal tyre force as a function of vertical load. Only one of the models is presented here but the results are also compared with the results obtained from the other models and with the measured rolling resistance in section 3.2.

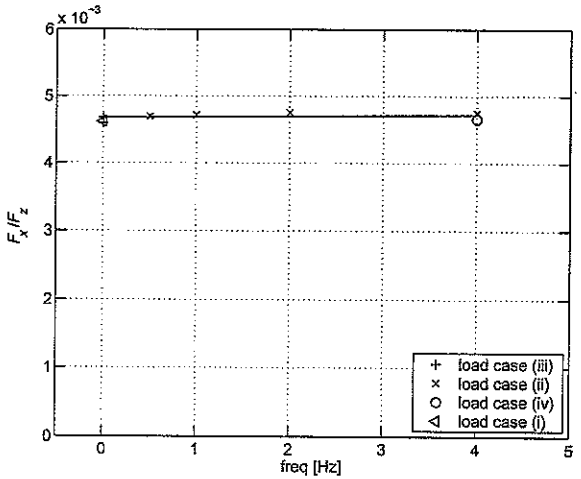

Figure 2. Rolling-resistance coefficient versus frequency of harmonic vertical force with mean value at start close to 35 kN, for 385/65R22.5 tyre at 9.4 bar and 40 km h^{-1} [7].

3.1 *Pacejka's transient tyre model*

In his book on tyre dynamics, Pacejka [9] devoted one chapter to the application of single-contact-point transient tyre models, where the response of the axle forces f_x and f_z to in-plane axle motions (x, z), road waviness and tyre non-uniformities is considered. The relationship between normal load f_z and radial tyre deflection ρ_t is simplified using the radial stiffness C_{Fz} ($f_z = C_{Fz}\rho_t$). The equations have been derived in detail by Pacejka [9]; so only a brief outline is presented here.

The variations in the effective rolling radius r_e with respect to tyre deflection ρ_t and tread depth d_t define two gradients $\eta = -(\partial r_e/\partial \rho_t)$ and $\varepsilon = -(\partial r_e/\partial d_t)$. A value of approximately 0.1 for η for radial tyres and 0.4 for bias-ply tyres is recommended [9]. In order to perform a linear analysis, small deviations (indicated with a tilde) from the undisturbed condition (indicated by an additional subscript 0) are assumed.

Variations in the free radius r_f along the circumference of the tyre due to variations in the carcass radius r_c and other variations in the tread thickness d_t are also considered. The horizontal in-plane tyre force in the contact patch has three components: the horizontal component of the normal load, the variation in the rolling resistance and the longitudinal force response to the variation in the wheels longitudinal slip.

The variation in the rolling resistance force is assumed to be directly transmitted to the tread through changes in the vertical load, which result from variations in the tyre deflection and possibly changes in the radial stiffness along the circumference of the tyre. The variations in tyre deflection result from vertical wheel displacement, tyre out-of-roundness and road height changes.

By combining all these effects and linearizing the relevant equations, a general expression for the small variations in the horizontal tyre force can be derived in the frequency domain. From this general expression, individual contributions can be evaluated. However, it is worth noting that there is no physical energy loss mechanism associated. In the case of the frequency response to axle motions on smooth and level ground, the following are obtained:

$$\frac{\tilde{F}_x}{Z} = -A_r C_{Fz} - \frac{\eta C_{F\kappa}}{r_0}\frac{2\zeta i\nu}{1-\nu^2+2\zeta i\nu}, \tag{2a}$$

the non-dimensional frequency

$$\nu = \frac{\omega}{\omega_{\Omega_0}}, \tag{2b}$$

the speed-dependent damping ratio

$$\zeta = \frac{1}{2}\frac{I_w V_x}{C_{F\kappa} r_0^2}\omega_{\Omega_0}, \tag{2c}$$

and the natural frequency of the tyre–wheel rotation with respect to the contact patch

$$\omega_{\Omega_0} = \left(\frac{C_{Fx} r_0^2}{I_w}\right)^{1/2}, \tag{2d}$$

where capital letters indicate the Laplace transform of the corresponding variables, z being the vertical axle displacement. The parameters are as follows: A_r, rolling resistance coefficient; $C_{F\kappa}$, longitudinal creep coefficient; r, tyre's loaded radius; I_w, wheel's polar moment of

inertia; C_{Fx}, longitudinal tyre stiffness. In order to compare the model predictions with the experimental results, the mean rolling resistance needs to be calculated:

$$\overline{f_x} = -\frac{f_{z0}}{2\pi}\int_0^{2\pi}\left[A_r + \frac{\eta C_{F\kappa}}{r_0 C_{Fz}}\,\mathrm{Im}\left(\frac{2\zeta \mathrm{i}\nu}{1-\nu^2+2\zeta \mathrm{i}\nu}\right)\left|\frac{\tilde{f}_z(t)}{f_{z0}}\right|\sin(\omega t)\right]\mathrm{d}(\omega t). \quad (3)$$

The contribution of the second term in the integral in equation (3) is zero because the sine function is integrated over a period. Therefore, the mean rolling resistance is equal to the static rolling resistance ($\overline{f_x} = -A_r f_{z0}$) and the dynamic load has no effect, as observed experimentally [7].

Appropriate numerical values must be chosen for the various parameters: A_r, C_{Fx}, $C_{F\kappa}$, C_{Fz}, η and r_0. The radial tyre stiffness C_{Fz} is the dynamic tyre stiffness: this can be derived either using a mass–spring–dashpot arrangement ($k_t + c_t \mathrm{i}\omega - m_t\omega^2$), or from a flexible ring model $K_T(\omega)$ [12], using appropriate boundary conditions. A_r is the static rolling resistance coefficient as measured by Popov *et al.* [7]. The longitudinal creep coefficient $C_{F\kappa}$ was measured [13] as a function of the vertical load for a similar tyre (295/75R22.5). Thorvald [14] measured the longitudinal tyre stiffness as a function of the vertical load and inflation pressure for a similar heavy-vehicle tyre (315/80R22.5). The value for C_{Fx} was chosen on the basis of his results, while η was taken to be 0.1, according to Pacejka's recommendations. The static loaded tyre radius r_0 can be calculated using the free undeformed tyre radius and the static tyre stiffness. The numerical values used for simulations are summarized in table 1.

The amplitude of the rolling resistance coefficient as a function of frequency is shown in figure 3, using both the dynamic tyre stiffness from the flexible-ring model and a mass–spring–dashpot arrangement. The model includes both the static and the dynamic components. At low frequencies, both plots exhibit the same static rolling resistance, corresponding to the value chosen for A_r. The results show a resonance at approximately 17 Hz, which corresponds to the natural frequency ω_{Ω_0} of the tyre–wheel rotation with respect to the contact patch. The axle hop vibration mode is also shown at approximately 25 Hz. This is higher than normally observed (10–15 Hz) because the model only includes the wheel and the tyre, but not the axle. In both cases, the rolling resistance returns to the static value once past the resonances, as expected.

The results are highly dependent on the value of η chosen, which also has a great degree of uncertainty associated. The value of 0.1 in the literature seems to be based on car (radial) tyres. It is possible that truck tyres, because of their different design and substantially higher loads, will exhibit different values of η. The effect of η on rolling resistance is considered in figure 4, using the dynamic tyre stiffness from the flexible ring model. The results show that increasing η has the effect of increasing the amplitude of both resonances.

Table 1. Parameter values for the adopted model using a Dunlop tyre SP241 385/65R22.5.

η	A_r	$C_{F\kappa}$ (N)	C_{Fx} (N m^{-1})	r_f (m)	r_e (m)	V_x (km h^{-1})	R_D (m)
0.1	6.41×10^{-3}	2.21×10^5	7.66×10^5	0.536	0.525	40	1.5

	r_0 (m)	ω_{Ω_0} (rad s^{-1})	ζ (%)
Flexible-ring model	0.512	106.5	5.22
Mass–spring–dashpot arrangement	0.494	102.7	5.41

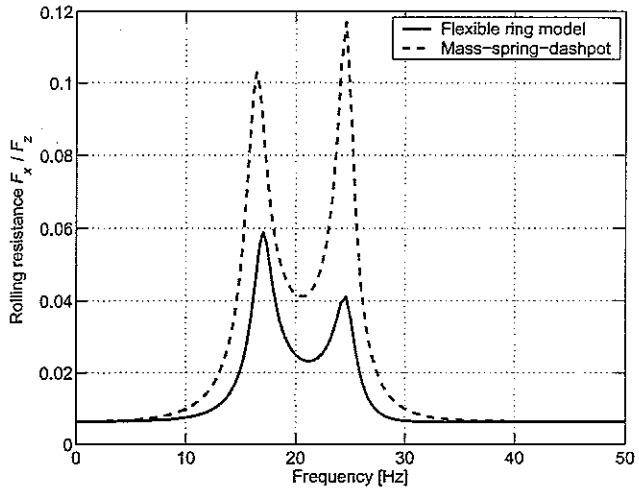

Figure 3. Amplitude of dynamic rolling resistance from the model.

The model gives a constant mean rolling resistance upon which the dynamic loading has no effect, which corresponds to what was observed experimentally [7]. It is able to model both the vertical dynamics of the tyre and the mechanics in the contact patch and includes a static and a dynamic component. However, its shortcoming is the lack of a physical mechanism to model the static rolling resistance, which leaves no choice but to adopt A_r to match the measured static rolling resistance.

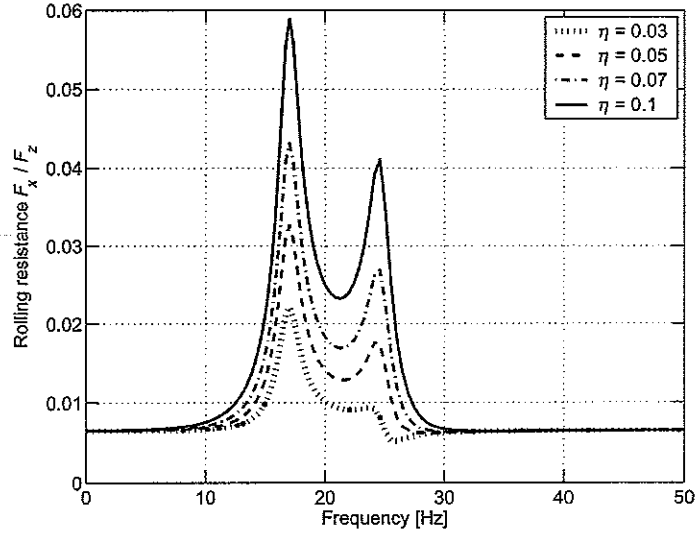

Figure 4. Influence of η on the amplitude of dynamic rolling resistance.

3.2 *Discussion of other models*

In order to decide which model is best suited to rolling resistance calculations under a dynamic vertical load, the amplitudes predicted from three models are compared in figure 5. For further details of the Segel–Lu model, as well as Zegelaar's model, the reader should refer to [11].

At low frequencies (figure 5(b)), all the models considered agree well, except the Segel–Lu model combined with the dynamic tyre stiffness from the flexible ring model. This is due to a discrepancy in the static tyre stiffness predicted by the flexible-ring model and the mass–spring–dashpot arrangement. As the frequency increases, the axle hop vibration is shown by

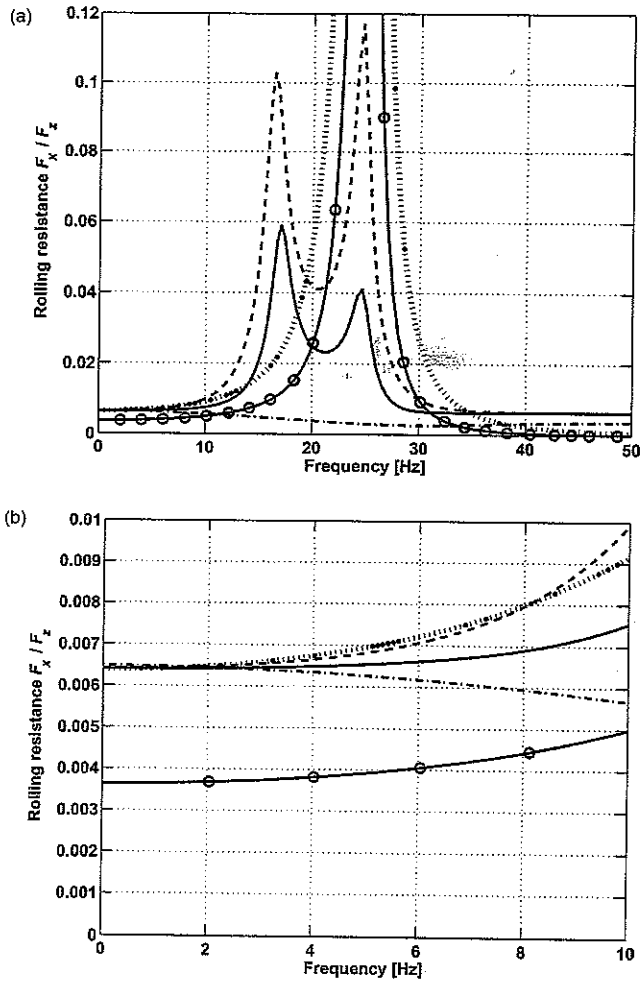

Figure 5. Comparison of rolling resistance amplitude under dynamic vertical load using three different models: Pacejka's model with flexible ring model (——), Pacejka's model with mass–spring–damper (– – –), Zegelaar's model (· – · – ·), Segel and Lu's model with flexible ring model (—◯—), Segel and Lu's model with mass–spring–damper (· · · · · ·). (a) Over a large frequency range; (b) at low frequencies.

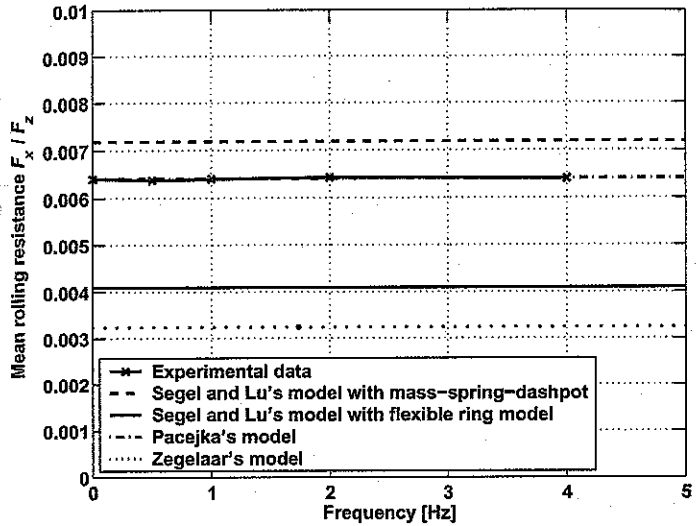

Figure 6. Comparison of mean rolling resistance with experimental data.

all models except Zegelaar's model. This is because Zegelaar's model does not include any vertical tyre stiffness; therefore no resonance occurs. Only Pacejka's model is able to predict the resonance due to the tyre–wheel rotation with respect to the contact patch. Zegelaar's model gives unlikely levels of rolling resistance at high frequencies, because of an exponential component in the mathematical formulation of the model [11].

In figure 6, the mean rolling resistance predicted by the three models is compared with the experimental data from Popov *et al.* [7] (which was corrected for the drum curvature by a factor $1 + (r/R_D)$ [2], where R_D is the drum radius). Only Pacejka's model is able to predict a mean rolling resistance equal to the measured value, but after selecting A_r appropriately. The Segel–Lu model gives a mean rolling resistance which is either too large (when using a mass–spring–dashpot arrangement) or too small (when using the dynamic tyre from the flexible-ring model). Zegelaar's model gives a mean rolling resistance half the measured value. This is due to an exponential component in the mathematical formulation of the model (see [11] for further explanation).

Overall, Pacejka's model is the only approach able to match the experimental results (at low frequencies) and to predict the important features of tyre dynamics and tyre–road contact mechanics. It also takes into account the fact that the vertical load consists of a static component and a dynamic component superimposed on it. Finally, it is the only model for which the amplitudes at high frequencies return to the static value corresponding to steady rolling. There is some doubt as to the appropriate value for η but, even when using directly the available value from the literature on car tyres, the results remain reasonable.

4. Conclusions

(1) Three tyre models were compared for the prediction of the rolling resistance under a dynamic vertical load. The model that gave the best results [9] was detailed.

(2) A critical comparison of the models showed that they agree reasonably well at low frequencies (0–10 Hz) but exhibit very different characteristics at higher frequencies (10–50 Hz).
(3) Pacejka's model was found to be mostly appropriate for calculating the rolling resistance under a dynamic vertical load, based on the available experimental data, despite the lack of a physical mechanism for describing the static rolling resistance.
(4) In order to make a more definite recommendation, more experimental data would be required at higher frequencies. However, it was noted that reliably generating a dynamic vertical load above 6 Hz is difficult, which makes the validation of a tyre model at higher frequencies challenging.

Acknowledgements

This project was funded by the UK Engineering and Physical Sciences Research Council and Dunlop Tyres Ltd. The authors are grateful to Dr D.J. Cole from the University of Cambridge for his valuable contributions and suggestions. The authors also wish to thank Mr C.B. Winkler from UMTRI for the data that he provided, as well as Dr D. Cebon from the University of Cambridge for his help and advice.

References

[1] Schuring, D.J. and Redfield, J.S., 1982, Effect of tire rolling loss on fuel consumption of trucks. SAE paper 821267, Society of Automotive Engineers, New York, pp. 4086–4096.
[2] Schuring, D.J., 1980, The rolling loss of pneumatic tires. *Rubber Chemistry and Technology*, **53**(3), 600–727.
[3] Popov, A.A., Cole, D.J., Cebon, D. and Winkler, C.B., 1999, Energy loss in truck tyres and suspensions. In *Proceedings of the 16th IAVSD Symposium on the Dynamics of Vehicles on Roads and Tracks* Pretoria, South Africa, *Vehicle System Dynamics, Supplement*, **33**, 516–527.
[4] Segel, L. and Lu, X.P., 1982, Vehicular resistance to motion as influenced by road roughness and highway alignment. *Australian Road Research Board*, **12**(4), 211–222.
[5] Klingbeil, W.W., 1980, Theoretical prediction of test variable effects, including twin-rolls, on rolling resistance. SAE paper 800088, Society of Automotive Engineers, New York, pp. 1–25.
[6] Klingbeil, W.W., Hong, S.W., Kienle, R.N. and Witt, H.W.H., 1983, Theoretical and experimental analysis of dual-compound tread designs for reduced rolling resistance. *American Chemical Society, Rubber Division Symposia*, **1**, 299–362.
[7] Popov, A.A., Cole, D.J., Winkler, C.B. and Cebon, D., 2003, Laboratory measurements of rolling resistance in truck tyres under dynamic vertical load. *Proceedings of the Institution of Mechanical Engineers, Part D: Journal of Automobile Engineering*, **217**(12), 1071–1079.
[8] Pottinger, M.G., Pelz, W., Tapia, G.A. and Winkler, C.B., 1996, A free-rolling cornering test for heavy-duty truck tires. *Tire Science and Technology*, **24**(2), 153–180.
[9] Pacejka, H.B., 2002, *Tyre and Vehicle Dynamics* (Oxford: Butterworth–Heinemann).
[10] Zegelaar, P.W.A., 1998, The dynamic response of tyres to brake torque variations and road unevennesses. PhD thesis, Delft University of Technology, Delft, The Netherlands.
[11] Miège, A.J.P. and Popov, A.A., 2004, Truck tyre modelling for rolling resistance calculations under dynamic vertical load. (Submitted).
[12] Gong, S., 1993, A study of in-plane dynamics of tyres. PhD thesis, Delft University of Technology, Delft, The Netherlands.
[13] Winkler, C.B., 1998, Private communication.
[14] Thorvald, B., 1998, On truck tyre modelling. PhD thesis, Kungl Tekniska Högskolan (Royal Institute of Technology), Stockholm, Sweden.

Vehicle System Dynamics
Vol. 43, Supplement, 2005, 145–155

Modelling of vibration damping in pneumatic tyres

ATANAS A. POPOV* and ZUNMIN GENG

School of Mechanical, Materials and Manufacturing Engineering, University of Nottingham, University Park, Nottingham NG7 2RD, UK

The paper deals with the measurement, identification and modelling of vibration damping in heavy vehicle tyres. Recent developments in vibration analysis are applied in order to extend the damping modelling to more general cases than viscous or hysteretic damping models based on a dissipation matrix. Both the general first-order state-space approach and the second-order small-damping method are critically reviewed. A general procedure for damping identification is developed and implemented. The only limitation to this procedure is that structural linearity and reciprocity should be satisfied; this has been adequately proven for pneumatic tyres. The best theoretical results have been achieved by assuming non-proportional viscous damping in the tyre and through the application of modal analysis techniques based on complex-valued modes.

Keywords: Pneumatic tyres; Damping identification; Modal analysis; Non-proportional viscous damping; Complex modes; Tyre modelling

1. Introduction

The interaction between a tyre and the road, together with the interaction between a tyre and the surrounding air, leads to a multitude of noises and vibrations [1]. Since tyre dynamics are central to the transmission and dissipation of vibrational and acoustical energy, one can reasonably argue that tyre damping is essential for the underlying physical phenomena. However, the role of tyre damping in vehicle dynamics is somewhat overshadowed by other factors which are thought to be of more importance. For example, the vehicle designer relies mostly on damping in the shock absorbers in the low-frequency range and on dissipation of sound energy in the vehicle body within the audible-frequency range.

A good balance in model complexity between a tyre and a vehicle is needed to obtain efficient and accurate vehicle simulations. It is relatively easy to measure or calculate the inertia and stiffness properties of a tyre; however, the accurate determination of damping parameters currently presents an unsolved problem.

Damping is the removal of energy from a vibrating system [2]. The energy lost is either transmitted away from the system by some mechanism of radiation or dissipated within the system. All structures exhibit vibration damping but, despite a large body of literature on the subject, damping remains one of the least well-understood aspects of vibration analysis.

*Corresponding author. Email: Atanas.Popov@Nottingham.ac.uk

Vehicle System Dynamics
ISSN 0042-3114 print/ISSN 1744-5159 online © 2005 Taylor & Francis
http://www.tandf.co.uk/journals
DOI: 10.1080/00423110500140765

It so happens that damping forces are usually small in magnitude when compared with other interactions in a mechanical system but play an important role in the dynamic response; yet their mathematical description remains much more complicated. There is a fundamental problem because it is not in general clear which state variables govern the damping forces.

A widely used damping model, originated by Lord Rayleigh [3], assumes that instantaneous generalized velocities are the only relevant state variables which determine the damping forces; this is the celebrated 'viscous damping' model. It leads to a description of damping behaviour by a dissipation matrix, directly analogous to the mass and stiffness matrices of structural mechanics. A step further in the idealization, also introduced by Rayleigh, is to assume the damping matrix to be a linear combination of the mass and stiffness matrices, the so-called proportional damping. Under this assumption the frequencies and modes of vibration for the system under investigation have real values. There is no obvious reason to expect physical systems to exhibit proportional damping, and complex modes of vibration should be regarded as the norm; complex modes of vibration arise even with viscous damping provided that it is non-proportional.

There is a variety of tyre models in the literature with different levels of complexity, ranging from a simple spring–damper element (single point contact) through flexible-ring-type models to detailed finite-element simulations (see [4] for an account). In all these models, when damping effects were included, they were almost invariably of the equivalent proportional viscous damping type. Moreover, damping values as high as 10% of critical damping have been reported and used for vehicle simulations [1, 5]. On the other hand, in studies mainly concerned with the performance of automotive suspensions, the whole amount of chassis damping was considered to arise from the shock absorbers under the assumption that tyre damping is much smaller in magnitude than suspension damping (see, for example, [6]). Other researchers in the area [7] disagreed with this assumption and argued that a separate consideration of tyre damping is essential because tyre damping is responsible for the coupling between sprung and unsprung mass motions at the wheel-hop frequency.

Assuming the damping matrix to be of non-proportional viscous type, then direct decoupling of the second-order differential equations of structural dynamics is impossible. Generally, the first-order state-space approach [8] becomes the only feasible method. Woodhouse [9] showed that, for *small* damping, models of damping can be obtained by using directly the second-order differential equations of structural dynamics, employing a first-order perturbation expansion based on the undamped modes and natural frequencies. A method was proposed to obtain damping models from complex mode shapes and frequencies of vibration [10], and the feasibility of this approach was demonstrated on idealized linear arrays of damped spring–mass oscillators. However, it was not clear whether this approach was applicable to experimental data obtained for complex real structures. This important issue is addressed here in an attempt to employ the new theoretical results to the pneumatic tyre.

2. Experimental measurements

A rig for tyre testing was designed, manufactured and commissioned (figure 1). The wheel was rigidly attached to a seismic table. The pneumatic tyre was only in contact with the wheel and could perform free vibrations in the frequency range of interest, up to 200 Hz. The experimental techniques employed were as follows: excitation by a shaker with a chirp-sweeping input [11], and measurement by accelerometer positioned at 16 equally spaced points along the central circumference of the tyre. During the measurements the tip of the drive rod and the accelerometer were glued to the surface of the tyre. The excitation was

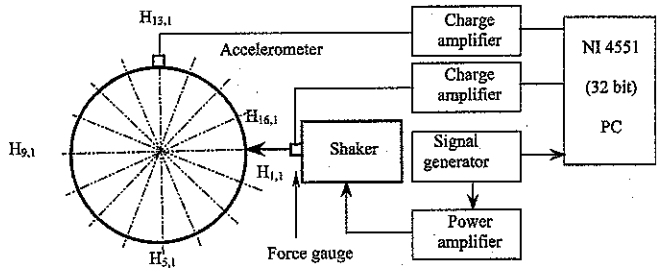

Figure 1. Modal testing set-up for a Dunlop truck tyre SP341 295/80R22.5: PC, personal computer.

applied in the radial direction, since only in-plane modes of tyre vibration were of interest. Simultaneous generation of excitation and acquisition of vibration response were performed through one National Instruments NI 4551 board [12]. The data were subsequently analysed with purpose-written programs in MATLAB [13].

The tyre used was a conventional single truck tyre Dunlop SP341 295/80R22.5, tested under different inflation pressures.

A large set of measurements was made to check for the linearity and reciprocity of tyre structure [14, 15]. Linearity was proven by exciting the tyre with harmonic loading of different magnitudes. Reciprocity was observed to a sufficient accuracy on the ensemble-averaged frequency response functions (FRFs). These initial checks for linearity and reciprocity justified a model with a symmetric damping matrix [9].

3. Procedures of modal analysis

In modal testing and analysis (see, for example, [8, 11]), any linear system with damping proportional only to velocities can be represented by a finite number N of degrees of freedom and a second-order differential equation of motion

$$[M]\{\ddot{x}(t)\} + [C]\{\dot{x}(t)\} + [K]\{x(t)\} = \{f(t)\}, \tag{1}$$

where $[M]$, $[C]$ and $[K]$ are the mass, dissipation (damping) and stiffness matrices respectively, $\{x(t)\}$ is the vector of generalized coordinates (radial tyre displacements in this particular case) and $\{f(t)\}$ is the vector of generalized forces driving the vibration (excitation force on the tyre by the shaker).

As a preliminary step towards the general analysis it can be assumed that the damping matrix of the tyre can be simultaneously diagonalized with the mass and stiffness matrices, meaning that damping is taken as proportional. In this case, a standard procedure is to transform equation (1) into the frequency domain and to decouple the equations of motion through a transformation of the generalised coordinates into modal coordinates by the $N \times N$ modal matrix $[\phi] = [\{\phi_1\}, \{\phi_2\}, \ldots, \{\phi_N\}]$. Here, the matrix columns represent the mode shapes of the undamped system scaled for unit mass, or $\{\phi_n\}^{\mathrm{T}}[M]\{\phi_n\} = [I]$ holds with $[I]$ as an $N \times N$ unit matrix. Under the assumption of proportional viscous damping, the FRFs commonly employed in modal testing and analysis [8, 11] are

$$H_{jk}(\omega) = \frac{X_j(\omega)}{F_k(\omega)} = \sum_{n=1}^{N} \frac{\phi_{jn}\phi_{kn}}{\omega_n^2 - \omega^2 + \mathrm{i}2\zeta_n\omega_n\omega}, \quad j,k = 1,\ldots,N. \tag{2}$$

References

[1] Mizuno, M., Takahashi, T. and Hada, M., 1998, Magic formula tyre model using the measured data of a vehicle running on actual road. *Proceedings of the 4th International Symposium on Advanced Vehicle Control*, Nagoya, Japan, 14–18 September.
[2] van Oosten, J. J. M., *et al.*, 1999, TIME, tyre measurements, forces and moments. Final Report, EC DG XII, Standards, Measurements and Testing, TNO, Delft, The Netherlands.
[3] Mizuno, M., *et al.*, 2003, The development of the tyre side force model considering the dependence of surface temperature of tyre. *Proceedings of the 18th IAVSD Symposium on the Dynamics of Vehicles on Roads and Tracks*, Atsugi, Kanagawa, Japan, 24–30 August (International Association for Vehicle System Dynamics).
[4] Bakker, E., Nyborg, L. and Pacejka, H. B., 1987, Tyre modelling for use in vehicle dynamics studies. SAE Paper 870495, Society of Automotive Engineers, New York.

Vehicle System Dynamics
Vol. 43, Supplement, 2005, 403–411

Taylor & Francis
Taylor & Francis Group

Vehicle–road interaction modelling for estimation of contact forces

N. K. M'SIRDI*†, A. RABHI†, N. ZBIRI† and Y. DELANNE‡

†Laboratoire de Robotique de Versailles, Université de Versailles, 10 avenue de l'Europe, 78140 Vélizy, France
‡Laboratoire Central des Ponts et Chaussées, Centre de Nantes, route de Bouaye, BP 4129-44341, 44 Bouguenais Cedex, France

The main objective of this paper deals with appropriate modelling (of a vehicle and the tyre–road contact) for online estimation of contact forces. This model will be helpful for trajectory monitoring, for steering control and also for diagnosis to avoid accidents or detection of oversteering or understeering situations. A robust observer is developed for adaptive estimation of the contact forces.

Keywords: Vehicle–road interaction model; Robust observers; Variable-structure systems; Sliding modes; Adaptive estimation and identification

1. Introduction

Recently, many analytical and experimental studies have been performed on the estimation of friction and contact forces between tyres and road. The latter affect the vehicle performance and behaviour properties. Thus for the analysis of vehicles and road safety it is necessary to take into account the contact force characteristics. However, forces and road friction are difficult to measure directly and complex to represent precisely by some deterministic equations.

The tyre models encountered are complex and depend on several factors (such as load, tyre pressure and environmental characteristics). This makes the forces and parameters difficult to estimate online, for vehicle control applications, detection and driving monitoring and surveillance. In the literature, their values are often deduced using some experimentally approximated models [1–3]. Knowledge of the tyre forces is essential for advanced vehicle control systems such as antilock braking systems, traction control systems and electronic stability programs [4–6].

In this paper, modelling of the contact forces and interactions between a vehicle and road is studied with the objective of online force estimation by means of robust observers [7] coupled with a robust estimation of contact forces. We use a simple vehicle representation well coupled with an appropriate wheel–road contact model in order to estimate contact forces online. We propose an observer to estimate the vehicle state and an estimator for identification

*Corresponding author. Email: msirdi@lrv.uvsq.fr

Vehicle System Dynamics
ISSN 0042-3114 print/ISSN 1744-5159 online © 2005 Taylor & Francis
http://www.tandf.co.uk/journals
DOI: 10.1080/00423110500109380

of tyre forces. The designed observer is based on the sliding-mode approach [8]. The main contribution is the online estimation of the tyre force needed for control.

The paper is organized as follows: section 2 deals with modelling of the vehicle and contact. The design of the observer is presented in section 3 and some results about the states observation are presented in section 4. Some remarks and perspectives are given in the conclusion in section 5.

2. Vehicle dynamics and road interactions

In the literature, many studies deal with vehicle modelling [9, 10]. These are complex and nonlinear systems (figure 1). The complete models are difficult to use in control applications. Most applications deal with simplified and partial models [11, 12]. We propose to consider a model that takes into account the contact effects (longitudinal–lateral) as inputs for the vehicle dynamics.

2.1 *Model of vehicle dynamics*

The first part of the model considered here is known as the bicycle model [11, 12]. It represents the longitudinal, lateral and yawing motions and the wheels' rotational motion. The two front wheels are grouped into one equivalent and similarly for the two rear wheels. We derive this simplified expression (figure 2) under the following assumptions.

(i) The epicentre is assumed to be at the road level.
(ii) The roll, pitch and vertical motions are neglected.
(iii) The road is assumed to be perfectly flat.
(iv) The influence of aerodynamic side forces is neglected.

In what follows, the subscripts f and r denote the front and rear wheels respectively. The resulting equations of the simplified vehicle model are

$$\begin{aligned} m\dot{V}_x &= F_{xf}\cos(\delta_f) - F_{yf}\sin(\delta_f) + F_{xr}, \\ m\dot{V}_y &= F_{xf}\sin(\delta_f) + F_{yf}\cos(\delta_f) + F_{yr}, \\ J_z\ddot{\psi} &= F_{xf}l_f\sin(\delta_f) + F_{yf}l_f\cos(\delta_f) - l_rF_{yr}. \end{aligned} \tag{1}$$

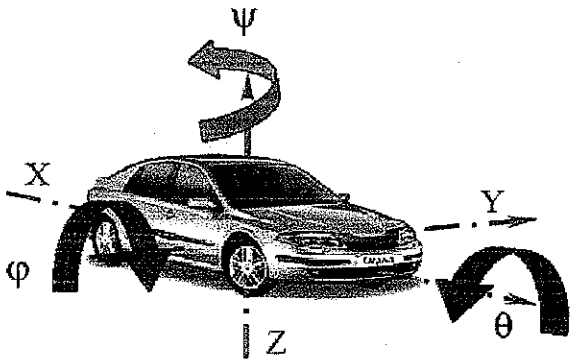

Figure 1. Vehicle reference coordinate system.

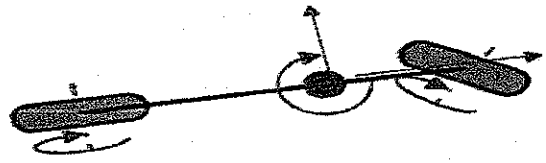

Figure 2. Bicycle model

F_{xf} and F_{yf} denote the longitudinal and the lateral forces respectively on the front wheels. F_{xr} and F_{yr} denote the longitudinal and the lateral forces respectively on the rear wheels. We note by δ_f the front-wheel steer angle ($\delta_r = 0$). The parameters l_r and l_f denote the distance between the centre of gravity of the vehicle and the front and the rear axis respectively. The wheel angular motion is given by

$$\dot{\omega}_f = \frac{1}{J_f}(T_f - r_f F_{xf}), \tag{2}$$

$$\dot{\omega}_r = \frac{1}{J_r}(T_r - r_r F_{xr}). \tag{3}$$

$\omega_f = \dot{\alpha}_f$ and $\omega_r = \dot{\alpha}_r$ are the rotation velocities of the front and rear wheel respectively. r_f and r_f denote the dynamic rays (front and rear respectively). J_f and J_r denote the inertias of the front and the rear wheels respectively. We denote by T_f and T_r the motor torques applied on the front and rear wheels respectively.

Coupling dynamic equations with an appropriate force description is a fairly good representation of the vehicle behaviour. The model considered in equations (1)–(3) needs to be completed by adding the interactions between the road and the wheels.

2.2 *Modelling of tyre contact*

Several models have been proposed for tyre contact. Most of these are empirical and depend on experimental parameters and measurement conditions. The motivation of these studies was to improve understanding of the tyre behaviour with respect to experimental results and then to include it in vehicle dynamic simulations. As an example, the most popular model is that of Pacejka and Besseling [13], namely the '*magic formula*' model. We can cite also as examples the *coefficient-of-longitudinal-friction model* [14] or the model of Gipser *et al.* [15]. Other models are based on expression of the distortions of the tyre and forces (static). The analytical models use a mechanical interpretation of the distortions of the tire and are based on elasticity [1, 6]. Recently many studies have considered the behaviour of the tyre in rapid transient manoeuvres such as cornering on uneven roads, brake torque variation and oscillatory steering. These studies deal with transients in tyre force and use the concept of relaxation length to take into account the deformations in the contact patch which are responsible for the lag in the response to lateral and longitudinal slip. The concept of relaxation length has been formulated particularly for the lateral dynamics to model transient tyre behaviour. This concept has been adapted for longitudinal dynamics. Pure longitudinal slip can be represented by a first-order relaxation. The slip stiffness is defined as the local derivative of the stationary tyre force–slip characteristic (figure 3): $C_x = \partial F/\partial s$.

2.2.1 Lateral dynamics and transient phenomenon. The dynamic behaviour of the transverse distortion has been the subject of several studies [1, 13, 16]. Pacejka and Besseling [13] described, by a first order model, the variations in the lateral strength and the moment of

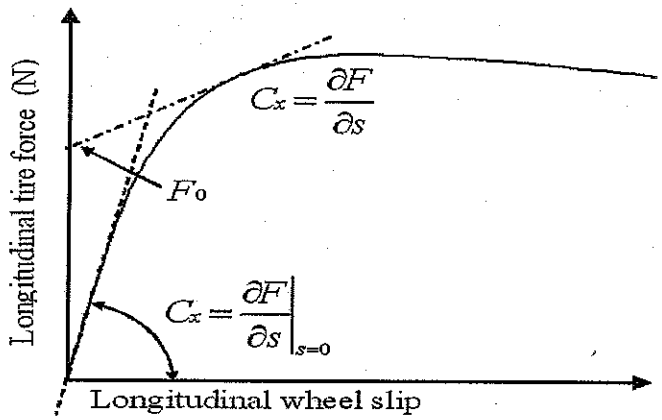

Figure 3. Force–slip characteristic

auto-alignment in the presence of weak values of the slip angle, while using the notion of the relaxation length. To illustrate the concept of the relaxation length, let us consider the dynamic variations in lateral strength F_y in the case of weak rates of slip. Suppose that the variation in the vertical strength is weak or that the force derivative is null: $\dot{F}_z = 0$. Then the variation in F_y is associated with a variation in the lateral speed of the contact point represented mainly by V_{cy}. So, to describe the transient, the variation in F_y is represented by a differential first-order equation as follows:

$$\sigma_{yi}\dot{F}_{yi} + V_{xi}F_{yi} = C_y V_y, \quad i = f, r \tag{4}$$

where C_y is the rigidity of the lateral slip and σ_y represents the relaxation length. This characterizes the behaviour around $F_y = 0$ at lateral force variation. We can extend the equation to the case of large slips to obtain

$$\sigma_{yi}\dot{F}_{yi} = -V_x(F_{yi} - F_{yi0}) + C_y V_y, \quad i = f, r \tag{5}$$

The unknown nominal parameters F_{yi0} are the intersection of the tangent line $\partial F_{yi}/\partial\lambda_{yi}$ and force axis F_{yi}.

2.2.2 Longitudinal dynamics and transient phenomenon. By analogy, the notion of relaxation length is used to describe the longitudinal dynamics. Clover and Bernard [3] presented the variations in the slip rate by a first-order differential equation. The longitudinal variation can be represented by the first-order model as follows: during the braking,

$$\sigma_{xi}\dot{F}_{xi} = -V_x(F_{xi} - F_{xi0}) + C_x(V_x - r_i\omega_i), \quad i = f, r$$

and, during the acceleration,

$$\sigma_{xi}\dot{F}_{xi} = -r_i\omega_i(F_{xi} - F_{xi0}) + C_x(V_x - r_i\omega_i), \quad i = f, r.$$

2.2.3 Contact equations. Finally, the model can be represented, during the acceleration phase, by

$$\begin{aligned}
\dot{F}_{xf} &= -\frac{V_x}{\sigma_{lf}}F_{xf} + \frac{V_x}{\sigma_{lf}}F_{xf0} + \frac{C_x}{\sigma_{lf}}V_x - \frac{C_x}{\sigma_{lf}}r_f\omega_f,\\
\dot{F}_{xr} &= -\frac{V_x}{\sigma_{lr}}F_{xr} + \frac{V_x}{\sigma_{lr}}F_{xr0} + \frac{C_x}{\sigma_{lr}}V_x - \frac{C_x}{\sigma_{lr}}r_r\omega_r,\\
\dot{F}_{yf} &= \frac{C_y}{\sigma_{tf}}V_y - \frac{V_x}{\sigma_{tf}}F_{yf} + \frac{V_x}{\sigma_{tf}}F_{yfo},\\
\dot{F}_{yr} &= \frac{C_y}{\sigma_{tr}}V_y - \frac{V_x}{\sigma_{tr}}F_{yr} + \frac{V_x}{\sigma_{tr}}F_{yro}.
\end{aligned} \tag{6}$$

2.2.4 Vehicle–road interaction model. Let us define the following state variables. $x_1 = (x, y, \psi, \alpha_f, \alpha_r)^T$ is the position vector and $x_2 = (V_x, V_y, \dot{\psi}, \omega_f, \omega_r)^T$ is the velocity vector. The force vector is denoted $x_3 = (F_{xf}, F_{xr}, F_{yf}, F_{yr})^T$.

The model can then be written in the state form as follows:

$$\begin{aligned}
\dot{x}_1 &= x_2\\
\dot{x}_2 &= \Omega(U)x_3 + BU\\
\dot{x}_3 &= \Psi(x_2, x_3)\Theta
\end{aligned} \tag{7}$$

where

$$\Omega(U) = \begin{bmatrix}
\frac{\cos(\delta_f)}{m} & \frac{1}{m} & \frac{-\sin(\delta_f)}{m} & 0\\
\frac{\sin(\delta_f)}{m} & 0 & \frac{\cos(\delta_f)}{m} & \frac{1}{m}\\
\frac{l_f\sin(\delta_f)}{J_z} & 0 & \frac{l_f\cos(\delta_f)}{J_z} & \frac{-l_r}{J_z}\\
\frac{-r_f}{J_f} & 0 & 0 & 0\\
0 & \frac{-r_r}{J_r} & 0 & 0
\end{bmatrix}, \quad B = \begin{bmatrix}
0 & 0 & 0\\
0 & 0 & 0\\
0 & 0 & 0\\
0 & \frac{1}{J_f} & 0\\
0 & 0 & \frac{1}{J_r}
\end{bmatrix} \quad \text{and} \quad U = \begin{bmatrix}\delta_f\\ T_f\\ T_r\end{bmatrix}.$$

The regression matrix $\Psi(x_2, x_3)$ is defined as follows, with $A_1 = C_x x_{21} - x_{21}x_{31} - C_x r_f x_{24}$ and $A_2 = C_x x_{21} - x_{21}x_{32} - C_x r_r x_{25}$:

$$\Psi(x_2, x_3) = \begin{bmatrix}
A_1 & 0 & x_{21} & 0 & 0 & 0 & 0 & 0\\
0 & A_2 & 0 & x_{21} & 0 & 0 & 0 & 0\\
0 & 0 & 0 & 0 & C_y x_{22} - x_{33}x_{21} & 0 & x_{21} & 0\\
0 & 0 & 0 & 0 & 0 & C_y x_{22} - x_{34}x_{21} & 0 & x_{21}
\end{bmatrix}.$$

In the model expression, we can introduce the parameters $\Theta = (\theta_1, \theta_2, \theta_3, \theta_4, \theta_5, \theta_6, \theta_7, \theta_8)^T$ as follows:

$$\begin{aligned}
&\theta_1 = \frac{1}{\sigma_{lf}}, \quad \theta_2 = \frac{F_{xf0}}{\sigma_{lf}}, \quad \theta_3 = \frac{1}{\sigma_{lr}}, \quad \theta_4 = \frac{F_{xr0}}{\sigma_{tr}}, \quad \theta_5 = \frac{1}{\sigma_{lf}},\\
&\theta_6 = \frac{F_{yf0}}{\sigma_{tf}}, \quad \theta_7 = \frac{1}{\sigma_{tr}}, \quad \theta_8 = \frac{F_{yr0}}{\sigma_{tr}}.
\end{aligned}$$

3. Adaptive estimation of tyre forces

3.1 *Expression for the robust observer*

The state vector is $x = (x_1, x_2, x_3)$ and the output $y = x_2$ ($y \in \mathbb{R}^5$) is the vector of measured outputs of the system. To estimate both forces and velocities we propose the following observer based on the sliding-mode approach [1, 8]:

$$\begin{aligned} \dot{\widehat{x}}_2 &= \Omega(U)\widehat{x}_3 + BU + \mathbf{H}_2 \operatorname{sgn}(x_2 - \widehat{x}_2), \\ \dot{\widehat{x}}_3 &= \Psi(\widehat{x}_2, \widehat{x}_3)\Theta + \mathbf{H}_3 \operatorname{sgn}(x_2 - \widehat{x}_2), \end{aligned} \tag{8}$$

where $\widehat{x}_i$ represent the observed state vectors, $\widetilde{x}_2 = x_2 - \widehat{x}_2$ are $\widetilde{x}_3 = x_3 - \widehat{x}_3$ are the state estimation errors. The observer gains $\mathbf{H}_i$ and the unknown parameter vector Θ will be defined hereafter. The dynamics of the estimation errors can be written as

$$\begin{aligned} \dot{\widetilde{x}}_2 &= \Omega(U)\widetilde{x}_3 - \mathbf{H}_2 \operatorname{sgn}(\widetilde{x}_2), \\ \dot{\widetilde{x}}_3 &= \Psi(x_2, x_3)\Theta - \Psi(\widehat{x}_2, \widehat{x}_3)\widehat{\Theta} - \mathbf{H}_3 \operatorname{sgn}(\widetilde{x}_2). \end{aligned} \tag{9}$$

In this observer we consider in fact only estimation of x_2 and x_3 and the partial state x_1 can be obtained by integration of $\widehat{x}_2$. The estimation error will be bounded, owing to the integration constant.

3.2 *Convergence analysis*

In order to study the observer stability, let us consider first the following Lyapunov function:

$$V_2 = \frac{1}{2}\widetilde{x}_2^{\mathrm{T}} \cdot \widetilde{x}_2 \tag{10}$$

The time derivative of V_2 is given by $\dot{V}_2 = \widetilde{x}_2^{\mathrm{T}} \cdot \dot{\widetilde{x}}_2$. According to equation (9), we can write

$$\dot{V}_2 = \widetilde{x}_2^{\mathrm{T}} \cdot [\Omega(U)\widetilde{x}_3 - \mathbf{H}_2 \operatorname{sgn}(\widetilde{x}_2)] = \widetilde{x}_2^{\mathrm{T}} \cdot \Omega(U)\widetilde{x}_3 - \widetilde{x}_2^{\mathrm{T}} \cdot \mathbf{H}_2 \operatorname{sgn}(\widetilde{x}_2).$$

The involved forces are bounded, owing to limitation of the system power. The *a priori* estimation $\widehat{x}_3$ is also bounded. Then we can consider that $\|\widetilde{x}_3\| < \mu$; μ is a positive finite constant. By chosing a positive matrix $\mathbf{H}_2$ ($\mathbf{H}_2 > \mu\Omega$) we have $\dot{V}_2 < 0$; the surface $\widetilde{x}_2 = \mathbf{0}$ is then attractive, leading $\widetilde{x}_2$ to converge towards x_2 in a finite time t_0 [7, 8]. Moreover, on average we have $\dot{\widetilde{x}}_2 = \mathbf{0}\ \forall t > t_0$. Consequently we can deduce that, on average,

$$\Omega(U)\widetilde{x}_3 - \mathbf{H}_2 \operatorname{sgn}(\widetilde{x}_2) = \mathbf{0} \longrightarrow \widetilde{x}_3 = \Omega(U)^{+}\mathbf{H}_2 \operatorname{sgn}(\widetilde{x}_2), \tag{11}$$

where $\Omega(U)^{+}$ is a pseudo-inverse matrix. Now, let us consider a second Lyapunov function

$$V_3 = \frac{1}{2}\widetilde{x}_3^{\mathrm{T}} \cdot \widetilde{x}_3. \tag{12}$$

The time derivative is given by $\dot{V}_3 = \widetilde{x}_3^{\mathrm{T}} \cdot \dot{\widetilde{x}}_3 = \widetilde{x}_3^{\mathrm{T}} \cdot [\Psi(x_2, x_3)\Theta - \Psi(\widehat{x}_2, \widehat{x}_3)\widehat{\Theta} - \mathbf{H}_3 \operatorname{sgn}(\widetilde{x}_2)]$. From equation (9), $\dot{V}_3$ becomes $\dot{V}_3 = [\Omega(U)^{+}\mathbf{H}_2 \operatorname{sgn}(\widetilde{x}_2)]^{\mathrm{T}} \cdot [\Psi(x_2, x_3)\Theta - \Psi(\widehat{x}_2, \widehat{x}_3)\widehat{\Theta} - \mathbf{H}_3 \operatorname{sgn}(\widetilde{x}_2)]$ where $\left\|[\Psi(x_2, x_3)\Theta - \Psi(\widehat{x}_2, \widehat{x}_3)\widehat{\Theta}\right\| < \beta$. By considering the choice of gain $\mathbf{H}_3 \gg \beta$ we finally obtain $\dot{V}_3 < 0$. So $\widetilde{x}_3$ goes to zero in finite time t_1. Then, $\dot{\widetilde{x}}_3 \to \mathbf{0}$ therefore, $\Psi(x_2, x_3)\Theta - \Psi(\widehat{x}_2, \widehat{x}_3)\widehat{\Theta} - \mathbf{H}_3 \operatorname{sgn}(\widetilde{x}_2) \to \mathbf{0}$. Because $\widetilde{x}_2 = \mathbf{0}$ and $\widetilde{x}_3 = \mathbf{0}\ \forall t > t_1$, we then have $\Psi(x_2, x_3) = \Psi(\widehat{x}_2, \widehat{x}_3)$ and therefore $\Psi(x_2, x_3)(\Theta - \widehat{\Theta}) = \mathbf{H}_3 \operatorname{sgn}(\widetilde{x}_2)$.

So we can conclude that the parameters can also by retrieved by construction:

$$\Theta = \widehat{\Theta} + \Psi(x_2, x_3)^{-1}\mathbf{H}_3 \operatorname{sgn}_{\mathrm{eq}}(\widetilde{x}_2).$$

4. Simulation results

In this section, we give some results in order to test and validate our approach and the proposed observer. In the simulation, the forces are generated by use of the 'magic formula' tyre model.

The steering angle applied is shown in figure 4. Figures 5 and 6 show the convergence of the estimated state vectors to their actual value in finite time. In figure 7 we show the asymptotic

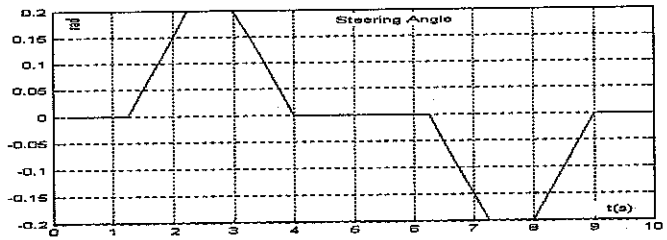

Figure 4. Steering angle.

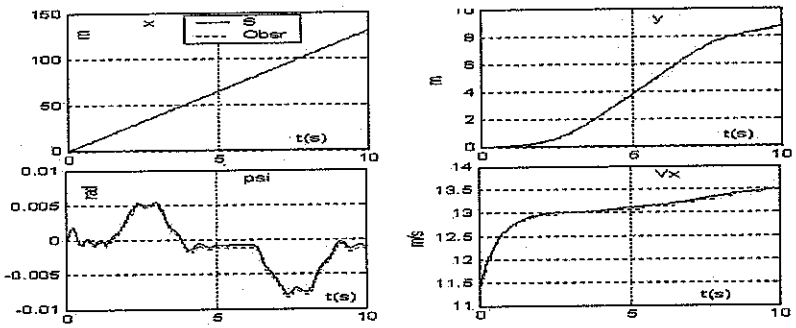

Figure 5. Estimated and measured states.

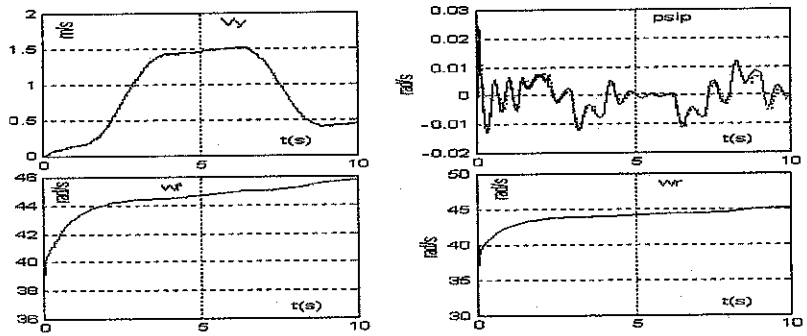

Figure 6. Estimated and measured states.

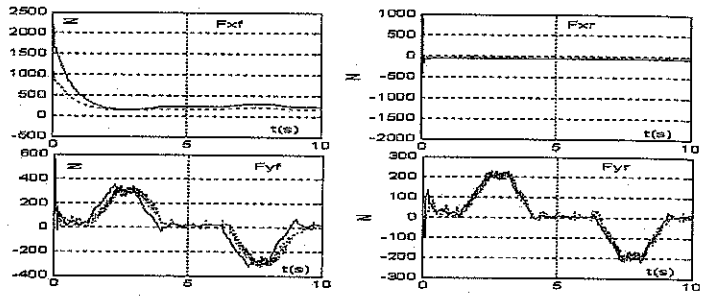

Figure 7. Estimated and measured forces.

convergence of the tyre force to actual values. The performance of the sliding-mode observer is satisfactory. The simulation results show that the adaptive observer is robust with respect to parameters and model uncertainties and to the changes in the road conditions.

5. Conclusion

In this paper, we have developed a new estimation method for a vehicle-dynamics-based sliding-mode observer and an adequate simplified model. Simulation results are presented to illustrate the ability of this approach to give estimation of both vehicle states and tyre forces. The robustness of the sliding-mode observer versus uncertainties in the model parameters has also been emphasized in simulation. This method will be applied to an instrumented vehicle.

References

[1] Pacejka, H.B., 1973, Simplified behaviour of steady state turning behaviour of motor vehilcles, part 2: stability of the steady state turn. *Vehicle System Dynamics*, **2**, 173–183.
[2] Liu, C.S. and Peng, H., 1996, Road friction coefficient estimation for vehicle path prediction. *Vehicle System Dynamics, Supplement*, **25**, 413–425.
[3] Clover, C.L. and Bernard, J.E., 1998, Longitudinal tire dynamics. *Vehicle System Dynamics*, **29**, 231–259.
[4] Drakunov, S., Ozguner, U., Dix, P. and Ashrafi, B., 1995, ABS control using optimum search via sliding modes. *IEEE Transactions on Control Systems Technology*, **3**, 79–85.
[5] Harned, J., Johnston, L. and Scharpf, G., 1969, Measurement of tire brake forces characteristics as related to wheel slip (antilock) control system design. *SAE Transactions*, **78**, 909–925.
[6] Dugoff, P.F.H. and Segel, L., 1970, An analysis of tire traction properties and their influence on vehicle dynamic performance. *SAE Transactions*, **3**, 1219–1243.
[7] Fridman, L. and Castanos, F., 2004, Integral sliding mode control design via Lyapunov methods for decentralized control. In: *Proceedings of the 43rd IEEE Conference on Decision and Control*, 2004 (New York: IEEE).
[8] Fridman, L. Sliding mode control for systems with fast actuators: singularly perturbed. In: X. Yu and J.-X. Xu, (Eds) *Variable Structure Systems: Toward the 21st century*, Lecture Notes in Control and Information Science, Vol. 274 (London: Springer).
[9] Venture, G., 2003, Identification des paramètres dynamiques d'une voiture. Thèse de Doctorat, L'Ecole Polytechnique de l'Université de Nantes, Institut de Recherch en Communications et cn Cybernétique de Nantes.
[10] Ramirez Mendoza, R.A., 1997, Sur la modélisation et la commande des véhicules automobiles. Doctorat, L'Institut National Polytechnique de Grenoble, 1997.
[11] Ackermann, J., 1997, Robust control prevents car skidding. *IEEE Control Systems Magazine*, **17**, 23–31.
[12] Lee, H. and Tomizuka, M. Adaptative vehicle traction force control for intelligent vehicle highway systems (IVHSs). *IEEE Transactions on Industrial Electronics*, **50**.
[13] Pacejka, H.B. and Besseling, I., 1997, Magic formula tyre model with transient properties. In: *Proceedings of the 2nd International Colloquium on Tyre Models for Vehicle Dynamic Analysis*, Berlin, 1997 (Lisse: Swets and Zeitlinger).

[14] Beurier, G. and Delanne, Y., 2000, Transposition de performances longitudinales de pneumatique – méthode de recherche statistique de relations entre les paramètres de modèles en vue de l'identification de ces paramètres. In: *Proceedings of the Conférence International Francophane d'Automatique*, Lille, France, 2000.
[15] Gipser, M., Hofer, R. and Lugner, P., 1997, Dynamical tyre forces response to road unevennesses. *Vehicle System Dynamics, Supplement*, **27**, 94–108.
[16] Pacejka, H.B., 1973, Simplified behaviour of steady state turning behaviour of motor vehilcles, part 1: handling diagrams and simple systems. *Vehicle System Dynamics*, **2**, 162–172.

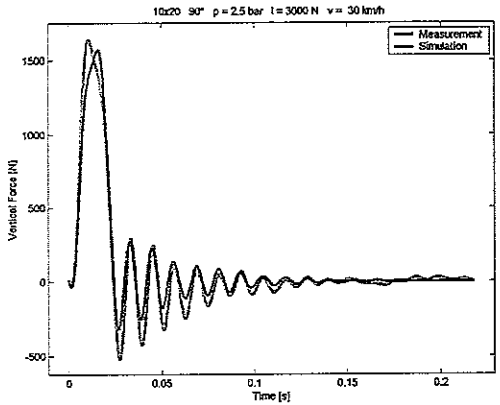

Figure 22. Cleat run result (F_z).

Lateral stiffness and contact geometry results are given in figures 15–17.

Pure-longitudinal slip and pure-lateral slip results are given in figures 18–20.

Cleat run results are given in figures 21 and 22.

5. Conclusion

The selected results effectively span the range of static, stationary and transient applications. Without showing all the identification results used, very good agreement could be reached for both the static and the transient behaviours. Both of these categories have a high impact on typical comfort and durability applications and are the main focus of the LMS CDTire model family. This is also reflected in the discussed parameter identification procedure, showing the applicability of the LMS CDTire Parameter Identification software with generally satisfactory results.

For the stationary tyre behaviour the generated results are also acceptable for typical comfort and durability applications. The accuracy for these slip simulations depends heavily not only on the tyre model and its parameters, but also on the test rig itself, in both the simulation and the measurement set-up.

Vehicle System Dynamics
Vol. 43, Supplement, 2005, 457–474

Taylor & Francis
Taylor & Francis Group

Identification of Pacejka's scaling factors from full-scale experimental tests

D. AROSIO*†, F. BRAGHIN‡, F. CHELI‡ and E. SABBIONI‡

†Pirelli Pneumatici S.p.A., Tyre and Vehicle System, Milan, Italy
‡Politecnico di Milano, Mechanical Engineering Department, Milan, Italy

A set of scaling factors has been introduced by Pacejka into his 'magic formula' tyre model to take into account the influence of a number of external overall parameters such as road roughness, weather conditions and suspension characteristics. These scaling factors are important for a correct prediction of tyre–road contact forces but are not a function of the tyre itself. From a different point of view, one could say that scaling factors should remain constant for different tyres on the same circuit, with the same weather conditions and with the same car. After having characterized different tyres through indoor tests (which do not consider external overall parameters) and after having identified Pacejka's coefficients with scaling factors assumed to be one, several outdoor experimental tests have been carried out to determine the influence of vehicle and road surface conditions on scaling factors. These experimental data allowed us to identify, through a minimization approach, the 'best' set of Pacejka's scaling factors for that vehicle and that tyre on that track. Scaling factors for the same track and vehicle but for different tyres were compared to check whether their values remained constant. All experimental data shown in this paper comes from tests carried out within the VERTEC project (vehicle, road, tyre and electronic control systems interaction: increasing active vehicle safety by means of a fully integrated model for behaviour prediction in potentially dangerous situations) (official contract G3RD-CT-2002-00805), a European funded research project that puts together knowledge from vehicle manufacturers (Volvo, Porsche and (CRF)), tyre manufacturers (Pirelli and Nokian Tyres), control logic manufacturers (Lucas Varity GmbH), road maintenance experts (CETE), transport research organizations (TRL) and (VTI) and universities (HUT) and (UNIFI)). The results shown in this paper are obtained by tests performed during tasks 2a (*Reference tyre characterizations and tests*) and 2b (*Development and validation of tyre–pavement interaction model*) of VERTEC project. The partners involved in these tasks are Pirelli, Nokian, Porsche, CRF, CETE, VTI, HUT and UNIFI.

Keywords: Tyre–road contact forces; 'Magic formula' tyre model; Pacejka's scaling factors; Indoor tyre testing; Outdoor tyre testing

1. Introduction

Pacejka's 'magic formula' (MF) tyre model is an empirical model; that is, it is a convenient set of analytical formulae that interpolates measured tyre data rather than modelling the tyre structure itself. To scale the formulae as a function of the vehicle's and/or the road characteristics and/or the weather conditions without changing the values of MF coefficients,

*Corresponding author.

Vehicle System Dynamics
ISSN 0042-3114 print/ISSN 1744-5159 online © 2005 Taylor & Francis
http://www.tandf.co.uk/journals
DOI: 10.1080/00423110500229683

26 scaling factors have been introduced.† Thus, the only feasible way to identify the values of scaling factors is to carry out full-scale outdoor experimental tests.

The identification of these scaling factors can be carried out by two methods.

(i) For each test, a different set of MF coefficients can be identified, forcing scaling factors to be equal to one; then, a test must be chosen as a reference; the scaling factors can thus be obtained by dividing the values of the MF coefficients identified in each test by the corresponding reference values.
(ii) A reference test is chosen; the values of the MF coefficients are identified only for this test (the scaling factors are assumed to be one); for all the other tests only the scaling factors are identified, assuming constant MF coefficient values.

Since different sets of MF coefficient values may all give good identification results (non-uniqueness of the identification procedure), method (i) may lead to high dispersion in the values of the scaling factors that is only due to the identification process. For this reason, method (ii) is chosen in the present work.

Scaling factors can be directly identified from experimental data if (and only if) tyre forces and moments are measured, for instance, using a dynamometric hub. Otherwise, an iterative identification procedure based on a multibody (MB) model is necessary to determine the scaling factors. However, uncertainties and approximations in the MB model may be interpreted as variation of scaling factors, thus giving rise to a higher dispersion in their values. In the present work, experimental tests were carried out with a dynamometric hub to avoid this problem.

As already stated, reference values of MF coefficients can be determined from any experimental test both outdoors and indoors. However, since outdoor tests are more affected by weather conditions, indoor tests are more highly respected. The identification of reference values of MF coefficients was therefore based on experimental tests carried out under laboratory conditions.

2. Experimental tests

The aim of the work is to investigate the influence of the road surface and weather conditions and of the test vehicle on the values of the scaling factors and to check whether their values are independent from the tyre. Thus, outdoor experiments, performed by (VTI) and Nokian Tyres for task 2a of the VERTEC project, were carried out using two different test vehicles (VTI's BV12 B and Nokian Tyres' test vehicles) at different speeds, equipped with five completely different passenger car tyres (different sizes, different characteristics, different wear conditions, new and worn, and built by different manufacturers, Nokian and Pirelli) on five different road surfaces (dry asphalt, wet asphalt, rough ice, smooth ice and snow). The tested passenger car tyres are described in table 1. In the following, every tyre will be referred to by the abbreviations given in table 1.

2.1 *Indoor experimental tests*

Indoor tests were carried out by Pirelli on MTS Flat-Trac® III, varying the radial load, the slip angle, the longitudinal slippage and the camber angle. During these tests, tyre contact forces (longitudinal force, lateral force, vertical force, overturning torque, spindle torque and self-aligning torque) as well as loaded radius, slip angle and longitudinal slippage were precisely

†In this work, MF tyre version 2002 is considered [2].

Table 1. Tested passenger car tyres.

Producer	Name	Abbreviation	Status	Measure	Description
Pirelli	P7 91 V	PAN	New	205 60 R15	All-season tyre
Pirelli	P7 91 V	PDN	New	195 65 R15	All-season tyre
Nokian	Hakka Q	NBN	New	205 60 R15	Winter tyre (studless)
Nokian	WR	NCN	New	205 60 R15	Central European winter tyre
Nokian	WR	NCW	Worn	205 60 R15	Central European winter tyre

measured. The testing conditions used to characterise the five tyres are shown in table 2. All tests were performed at 22 m s^{-1} and an inflation pressure of 2.2 bar.

Experimental test data are then used to identify the reference values of MF coefficients for the five tyres. During this identification procedure, based on a minimization approach, scaling factors are assumed to be constant and equal to one.

As an example, figure 1 shows the comparison between experimental data (dotted curves) and the fitted MF tyre model (solid curves) for combined-slip tests carried out at a vertical load 3500 N of for six different slip angles (±1°, ±3° and ±9°). A very good agreement between the experimental data and the fitted MF tyre model can be seen.

2.2 *Outdoor experimental tests*

VTI and Nokian Tyres performed outdoor tests, using their test vehicles, in order to investigate the tyres' behaviour on different road surfaces. In particular, five tracks were considered: dry asphalt, wet asphalt, smooth ice, rough ice and snow.

2.2.1 VTI outdoor tests. VTI's test vehicle BV12 B [3], shown in figure 2, is a two-axle Scania LB80 truck equipped with a test facility for passenger car tyres. The tyre under testing can be both driven and braked since its axle may be connected alternatively to the drive shaft of the truck via a continuously variable V-belt gear box and a two-step gearbox or to a disc brake. The two gearboxes allow constant- or variable-slip measurements in the

Table 2. Indoor tests performed by Pirelli (VERTEC project).

	Pure-longitudinal test				
Tyre	PAN	PDN	NCN	NCW	NBN
Slip ratio κ (%)	±50	±50	±50	±50	±50
Camber angle γ (deg)	−2, 0, 2	−2, 0, 2	0	0	0
Vertical load F_z (kN)	2, 3.5, 5	2, 3.5, 5	2, 3.5, 5	2, 3.5, 5	2, 3.5, 5
	Pure-cornering test				
Slip angle α (deg)	±15	±15	±15	±15	±15
Camber angle γ (deg)	−2, 0, 2	−2, 0, 2	0	0	0
Vertical load F_z (kN)	2, 3.5, 5	2, 3.5, 5	2, 3.5, 5	2, 3.5, 5	2, 3.5, 5
	Combined-slip test				
Slip ratio κ (%)	±50	±50	±50	±50	±50
Slip angle α (deg)	−9, −3, −6, −1, 1, 3, 6, 9	−9, −3, −6, −1, 1, 3, 6, 9	−9, −3, −1, 1, 6	−9, −3, −1, 1, 6	−9, −3, −1, 1, 6
Camber angle γ (deg)	−2, 0, 2	−2, 0, 2	0	0	0
Vertical load F_z (kN)	2, 3.5, 5	2, 3.5, 5	2, 3.5, 5	2, 3.5, 5	2, 3.5, 5

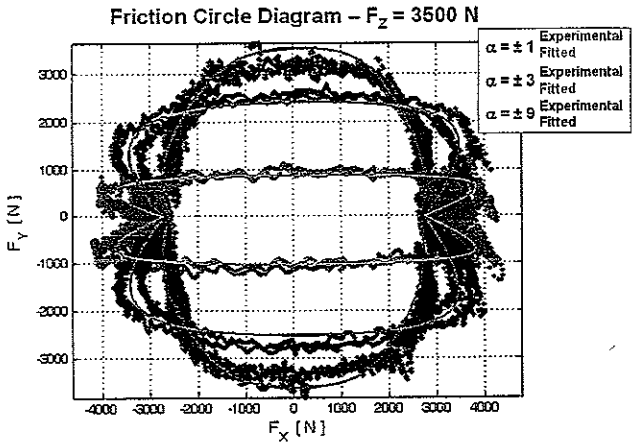

Figure 1. Comparison between experimental data and the fitted MF tyre model: friction circle diagram at a vertical load of 3500 N.

range 0–50%. The disc brake is normally used for locked-wheel braking tests but it could also be used for variable-braking-slip measurements. The slip angle of the tyre under testing can be continuously varied in the range $\pm 15°$ and combined testing conditions are allowed. The vertical load on the tyre under testing is applied by a hydraulic cylinder and can be varied from 1 to 6 kN. The maximum test speed is about 100 km h^{-1}. The test vehicle is equipped with a watering system that allows a water film of desired depth to be obtained. Tyre contact forces and moments are measured using a Kistler dynamometric hub.

Pure-braking tests, pure-cornering tests and combined-slip tests were performed with several wheel loads on dry asphalt, wet asphalt, smooth ice and rough ice. The different test conditions are described in table 3.

2.2.2 Nokian Tyres' outdoor tests. Nokian Tyres' test vehicle [4], shown in figure 3, is a four-wheel drive Volkswagen LT van equipped with two test facilities for passenger car tyres between the front and rear axles. The test facility on the right-hand side of the test vehicle allows both driving (through an hydraulic motor) and braking slip measurements to be carried

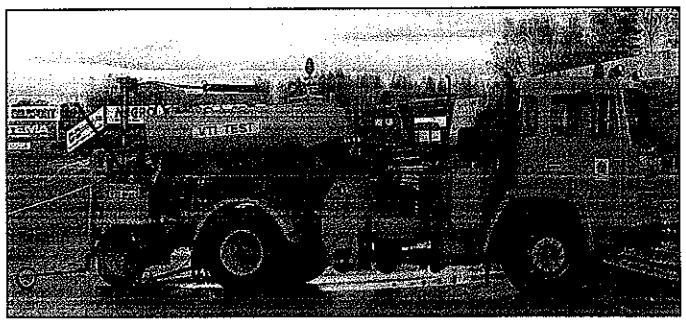

Figure 2. VTI's BV12 B test vehicle.

Table 3. Outdoor tests performed by VTI (VERTEC project).

Braking tests				
Road surface	Dry asphalt	Wet asphalt	Smooth ice	Rough ice
Slip ratio κ (%)	−100–0	−100–0	−100–0	−100–0
Vertical load F_z (kN)	2, 4, 6	2, 4, 6	3, 4, 5	3, 4, 5
Speed (km h^{-1})	80	80, 40	30	30
Pure-cornering tests				
Slip angle α (deg)	0–10	0–10	0–10	0–10
Vertical load F_z (kN)	2, 4, 6	2, 4, 6	3, 4, 5	3, 4, 5
Speed (km h^{-1})	80	80, 40	30	30
Combined-slip tests				
Slip ratio κ (%)	−100–0	−100–0	−100–0	−100–0
Slip angle α (deg)	1, 2, 5, 10	1, 2, 5, 10	1, 2, 5, 10	1, 2, 5, 10
Vertical Load F_z (kN)	2, 4, 6	2, 4, 6	3, 4, 5	3, 4, 5
Speed (km h^{-1})	80	80, 40	30	30

Figure 3. Nokian Tyres' test vehicle.

Table 4. Outdoor tests performed by Nokian Tyres (VERTEC project).

Braking tests		
Road surface	Smooth ice	Snow
Slip ratio κ (%)	−100–0	−100–0
Vertical load F_z (kN)	3, 4, 5	3, 4, 5
Speed (km h^{-1})	25	25
Pure-cornering tests		
Slip angle α (deg)	0–10	0–10
Vertical load F_z (kN)	3, 4, 5	3, 4, 5
Speed (km h^{-1})	25	25

out while that on the left-hand side allows only locked-wheel braking tests to be carried out. For the right-hand side test facility the longitudinal slip can be adjusted between −100% and 50%. The slip angles of both tyres under testing can be continuously varied between −5° and 15° and combined-testing conditions are allowed. The maximum slip angle frequency is 0.5 Hz. The vertical load on the tyres under testing is applied through hydraulic cylinders. The maximum test speed is about 100 km h^{-1}. Tyre contact forces and moments are measured using a Kistler dynamometric hub.

Pure-braking tests and pure-cornering tests were performed with several wheel loads on smooth ice and snow. The different test conditions are described in table 4.

3. Identification of Pacejka's scaling factors

Imposing constant values of MF coefficients (equal to the reference values identified from indoors tests), scaling factor values are identified through a minimization approach from outdoor experimental tests. The minimization algorithm is a subspace trust region method, based on the interior-reflective Newton method [5].

In the following, the results of the identification process for the scaling factors referring to pure longitudinal force, to pure cornering force and to combined slip forces, will be presented in terms of mean, maximum and minimum values as well as standard deviation for the five tyres considered.

The influence of the road surface, of the measurement vehicle and of the test vehicle speed on the scaling factors value will also be investigated.

3.1 *Pure-longitudinal-slip tests*

The scaling factors referring to the pure longitudinal slip [2] are $\lambda_{\mu x}$, λ_{Kx}, λ_{Cx}, λ_{Ex}, λ_{Hx}, λ_{Vx} and $\lambda_{\gamma x}$. However, $\lambda_{\gamma x}$ cannot be identified from the experimental data since nor are VTI's BV12 B and Nokian Tyres' test vehicle able to perform tests with camber angles different from zero.

Figures 4 and 5 show the comparison between experimental data ('averaged' measurement, dark grey curve) and fitted MF tyre model results (light grey curve) for a pure-braking test

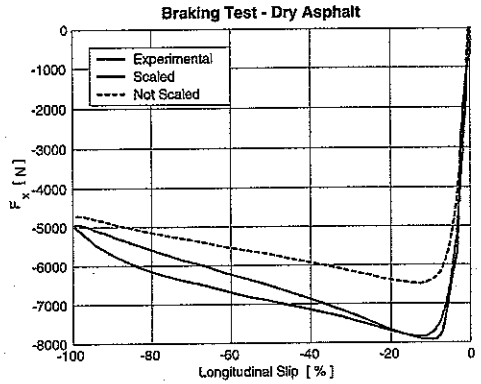

Figure 4. PAN tyre: comparison between experimental data ('averaged' measure) and fitted MF tyre model for a pure longitudinal slip test on dry asphalt with a vertical load of 6000 N.

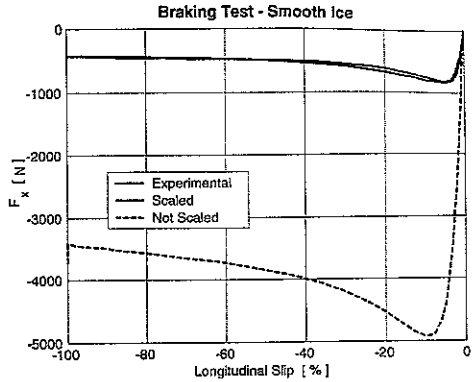

Figure 5. PAN tyre: comparison between experimental data ('averaged' measurement) and fitted MF tyre model for a pure longitudinal slip test on smooth ice with a vertical load of 5000 N.

with a vertical load of 6000 N carried out on dry asphalt by VTI with a PAN tyre and for a pure-braking test with a vertical load of 5000 N carried out on smooth ice by Nokian with the same tyre. Also the fitted MF tyre model results with unity scaling factors (black dashed curve) are shown.

The MF tyre model with scaling factor values different from one fits the experimental data well.

The influence of the road surface on the scaling factor values is investigated first. The mean (grey square), maximum and minimum (upper and lower limits of the vertical bars) values as well as standard deviation of the scaling factors on dry asphalt, wet asphalt, smooth ice and snow for the five considered tyres are shown in figures 6, 7, 8 and 9 respectively. As expected, the influence of the road surface is mostly seen on the peak friction scaling factor $\lambda_{\mu x}$, and on the stiffness scaling factor λ_{Kx}; the value of these scaling factors decrease on going from high friction (dry asphalt) to very low friction (smooth ice). It can be also noticed that the value of the scaling factors are very close to one on dry and wet asphalts, indicating that the equivalent road on MTS Flat-Trac® III has characteristics similar to real roads (micro-texture).

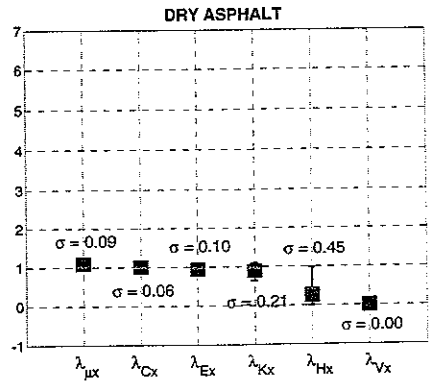

Figure 6. Pure-longitudinal slip tests: influence of the road surface, dry asphalt (VTI; 80 km h^{-1}).

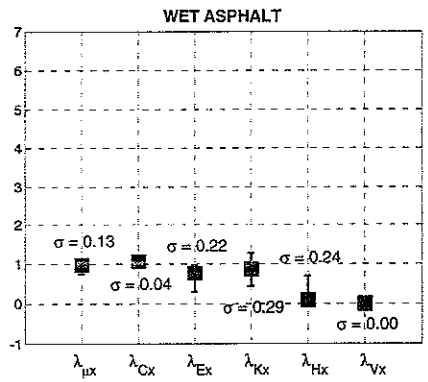

Figure 7. Pure-longitudinal-slip tests: influence of the road surface, wet asphalt (VTI; 80 km h^{-1}).

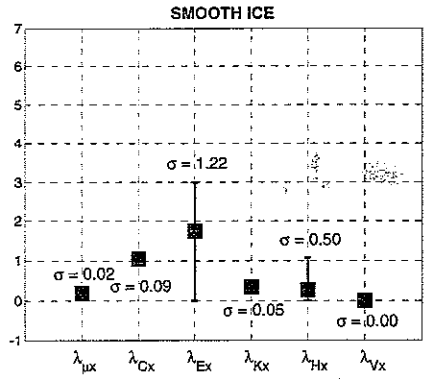

Figure 8. Pure-longitudinal-slip tests: influence of the road surface, smooth ice (VTI; 30 km h^{-1}).

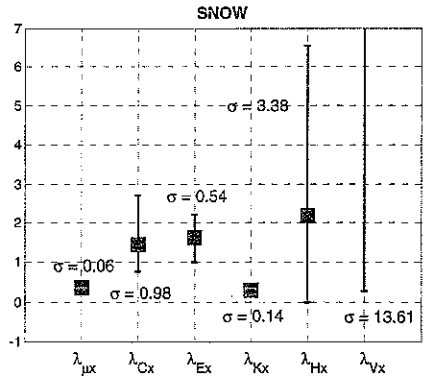

Figure 9. Pure-longitudinal-slip tests: influence of the road surface, snow (Nokian; 25 km h^{-1}).

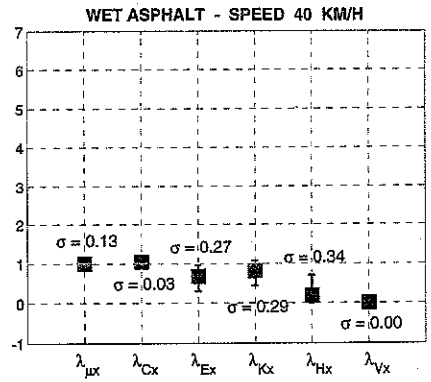

Figure 10. Pure-longitudinal-slip tests: influence of the test speed, 40 km h^{-1} (VTI; wet asphalt).

The dispersion of the scaling factors due to the road surface is very small in most cases, except for the vertical scaling factors λ_{Vx} and the horizontal shift scaling factor λ_{Hx}. This result can be explained by the fact that the identification was carried out considering only pure-braking conditions. To determine λ_{Hx} and λ_{Vx} properly, both driving and braking characteristics are necessary. Moreover shifts are usually very small. Therefore, to produce small changes in the shape of the tyre characteristics curves, relative changes in their values are significant. The shape factor λ_{Cx} is almost constant while the dispersion of the curvature scaling factor λ_{Ex} is very small on asphalt and increases on ice and snow.

The influence of the speed of the test vehicle is also analysed.

Figures 10 and 11 show the values of the scaling factors for pure-braking tests on wet asphalt identified from the tests performed by VTI at 40 km h^{-1} and 80 km h^{-1} respectively. Hardly any difference between the values of the scaling factors can be noticed. It can therefore be concluded that the speed of the test vehicle does not affect the values of the scaling factors.

Finally, the influence of the test vehicle is investigated. Figures 12 and 13 show the values of the scaling factors for pure-braking tests on smooth ice identified from the tests performed by

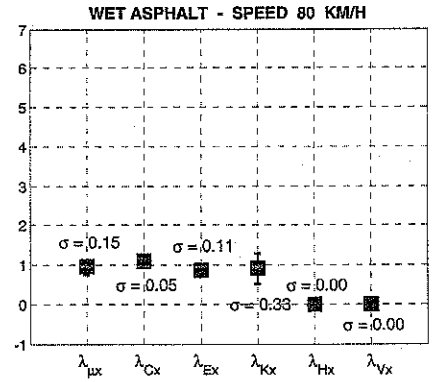

Figure 11. Pure-longitudinal-slip tests: influence of the test speed, 80 km h^{-1} (VTI; wet asphalt).

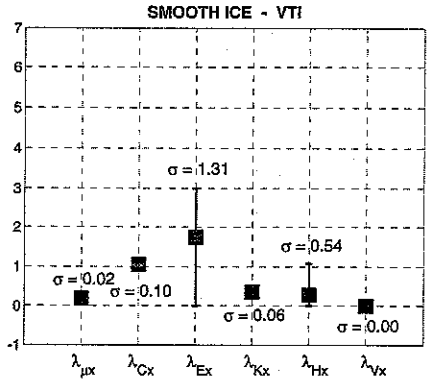

Figure 12. Pure-longitudinal-slip tests: influence of the test vehicle, VTI (smooth ice; 30 km h^{-1}).

VTI and Nokian Tyres respectively. The trend is very similar, except for the above-mentioned shift scaling factors and for the curvature scaling factor λ_{Ex}.

3.2 *Pure-lateral-slip tests*

The scaling factors referring to pure lateral slip [2] are $\lambda_{\mu y}$, λ_{Ky}, λ_{Cy}, λ_{Ey}, λ_{Hy}, λ_{Vy}, $\lambda_{\gamma y}$ and λ_{F_z0}. Since neither VTI's BV12 B nor Nokian Tyres' test vehicle are capable of performing tests with camber angles different from zero, $\lambda_{\gamma y}$ cannot be identified from the experimental data.

Figure 14 shows the comparison between experimental data ('averaged' measurement, dark grey curve) and fitted MF tyre model results (light grey curve) for a pure-cornering test at a vertical load of 6000 N carried out on dry asphalt by VTI with a PAN tyre while figure 15 is for a pure-cornering test with a vertical load of 5000 N carried out on smooth ice by Nokian Tyres with the same tyre.

In figures 16–19 the influence of the road surface on the scaling factor values is shown. As for the braking tests, $\lambda_{\mu y}$ and λ_{Ky} are significantly affected by the road surface conditions.

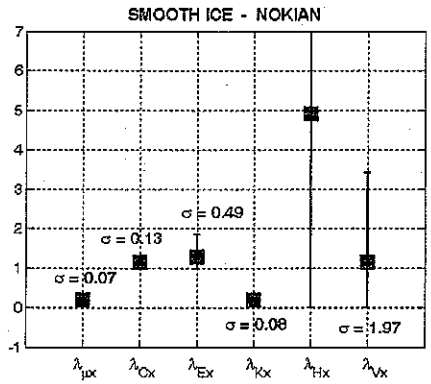

Figure 13. Pure-longitudinal-slip tests: influence of the test vehicle, Nokian Tyres (smooth ice; 25 km h^{-1}).

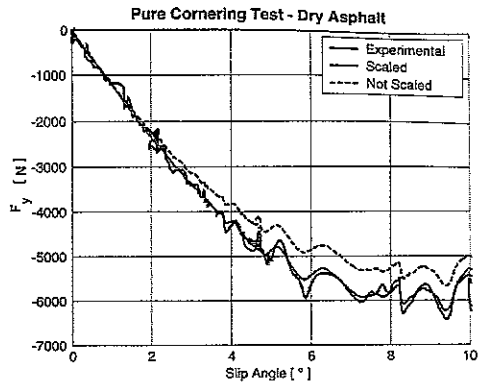

Figure 14. PAN tyre: comparison between experimental data ('averaged' measurement) and fitted MF tyre model for a pure-cornering test on dry asphalt with a vertical load of 6000 N.

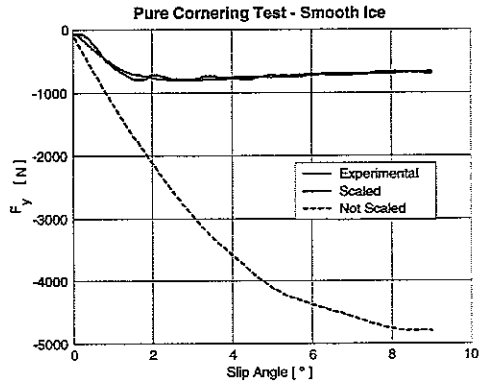

Figure 15. PAN tyre: comparison between experimental data ('averaged' measurement) and fitted MF tyre model for a pure-cornering test on smooth ice with a vertical load of 5000 N.

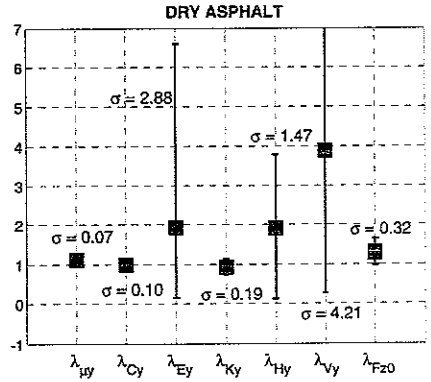

Figure 16. Pure-lateral-slip tests: influence of the road surface, dry asphalt (VTI; 80 km h^{-1}).

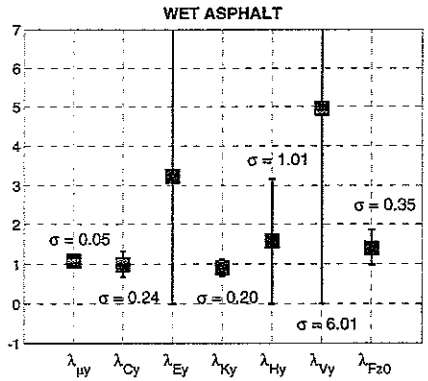

Figure 17. Pure-lateral-slip tests: influence of the road surface, wet asphalt (VTI; 80 km h^{-1}).

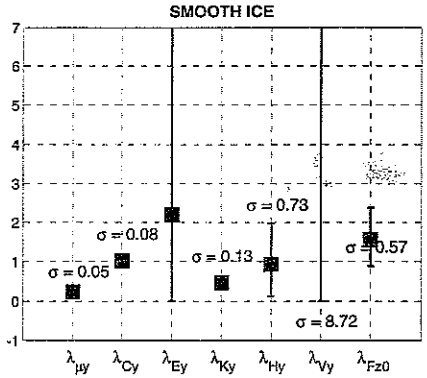

Figure 18. Pure-lateral-slip tests: influence of the road surface, smooth ice (VTI; 30 km h^{-1}).

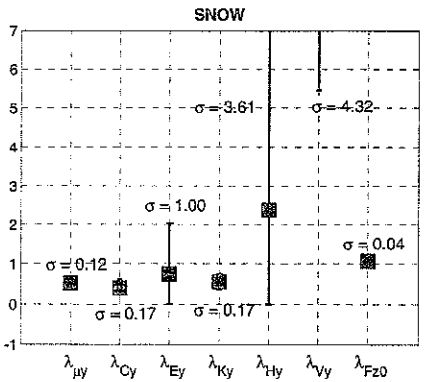

Figure 19. Pure-lateral-slip tests: influence of the road surface, snow (Nokian; 25 km h^{-1}).

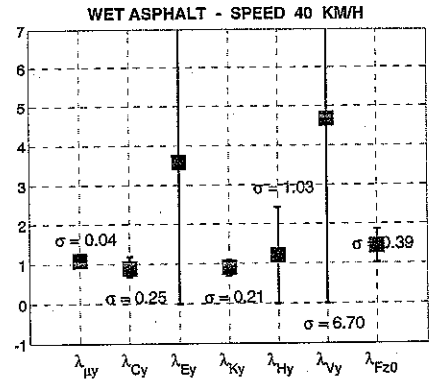

Figure 20. Pure-lateral-slip tests: influence of the test speed, 40 km h^{-1} (VTI; wet asphalt).

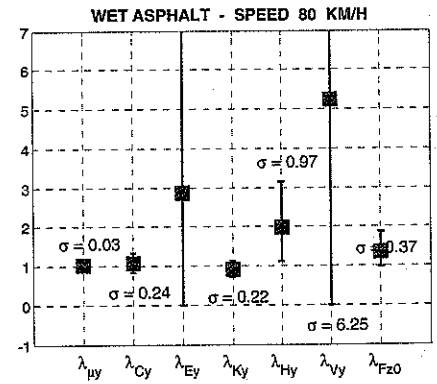

Figure 21. Pure-lateral-slip tests: influence of the test speed, 80 km h^{-1} (VTI; wet asphalt).

Moreover the shape scaling factor λ_{Cy} is significantly affected by the road surface. Again the dispersion of the scaling factor values is small, except for λ_{Hy}, λ_{Vy} and λ_{Ey}. As stated for the pure-braking tests, this is because the slip angle was varied only in the range 0–10°; that is, the tyres' behaviour was not investigated for negative slip angles (high dispersion in the values of the shift scaling factors) and for large slip angles (high dispersion in the values of the curvature scaling factors since the peak value of the lateral force may be outside the measurement range[‡]).

The influence of the speed of the test vehicle is assessed in figures 20 and figure 21. As for the braking tests, speed does not seem to have any influence on the scaling factor values (except for the shape scale factor λ_{Cy}).

Finally, the influence of the test vehicle is considered. As can be seen in figures 22 and 23, the test vehicle only effects the values of the shape scale factor λ_{Cy} and of the curvature scale factor λ_{Ey}.

[‡]For low-friction surfaces, such as smooth ice or snow, the dispersion of the λ_{E_y} scaling factor is smaller since the peak value of the lateral force is reached on the considered slip angle range.

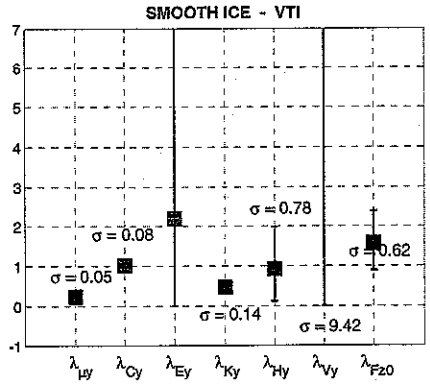

Figure 22. Pure-lateral-slip tests: influence of the test vehicle, VTI (smooth ice; 30 km h^{-1}).

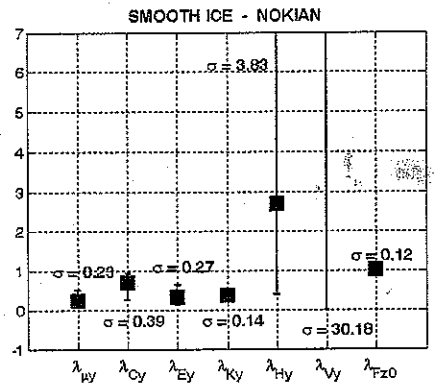

Figure 23. Pure-lateral-slip tests: influence of the test vehicle, Nokian Tyres (smooth ice; 25 km h^{-1}).

3.3 *Combined-slip tests*

The scaling factors referring to combined slip [2] are $\lambda_{x\alpha}$, $\lambda_{y\kappa}$ and $\lambda_{Vy\kappa}$. Since the identification of the scaling factors is carried out starting from the scaled MF coefficients and since the identification of pure-longitudinal and pure-cornering scaling factors gave good results, small variations are expected for the combined scaling factors.

Figures 24 and 25 show the comparison between experimental data and fitted MF tyre model for combined-slip tests carried out by VTI with a PAN tyre at a vertical load of 6000 N on dry asphalt, and by Nokian with the same tyre at a vertical load of 5000 N on smooth ice.

Figures 26–29 show the influence of the road on the value of combined-slip scaling factors. The influence of snow cannot be taken into account since Nokian Tyres did not carry out combined-slip tests.

As already said, combined-slip scaling factors are only slightly influenced by the road surface conditions. Moreover, dispersion is very small.

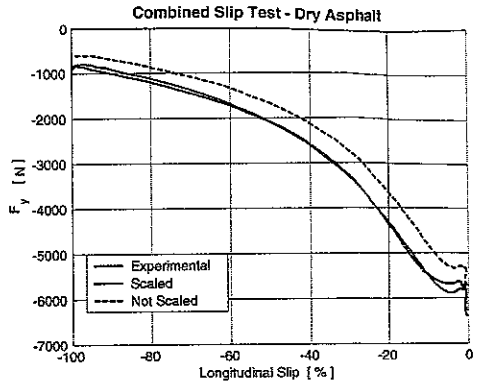

Figure 24. PAN tyre: comparison between experimental data ('averaged' measurement) and fitted MF tyre model for a combined-slip test on dry asphalt with a vertical load of 6000 N and a slip angle of 10°.

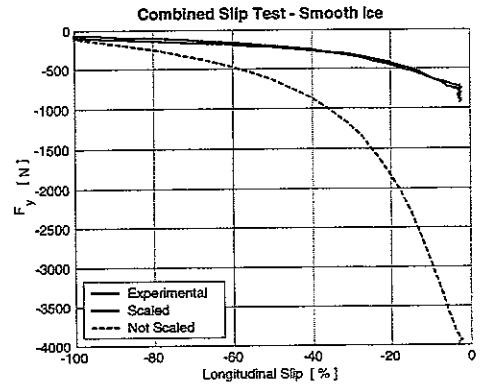

Figure 25. PAN tyre: comparison between experimental data ('averaged' measurement) and fitted MF tyre model for a combined-slip test on dry asphalt with a vertical load of 5000 N and a slip angle of 5°.

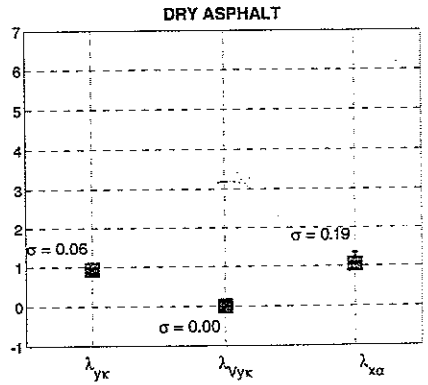

Figure 26. Combined-slip tests: influence of the road surface, dry asphalt (VTI; 80 km h^{-1}).

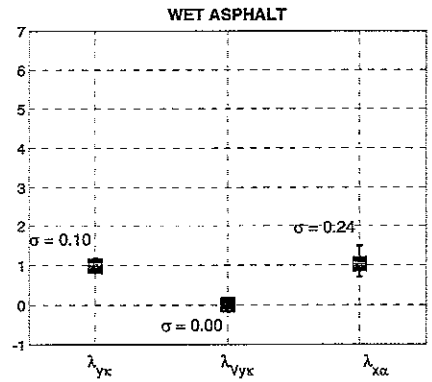

Figure 27. Combined-slip tests: influence of the road surface, wet asphalt (VTI; 80 km h^{-1}).

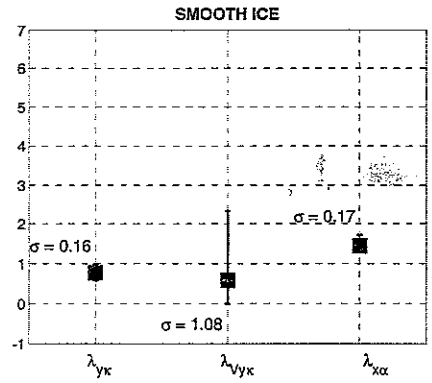

Figure 28. Combined-slip tests: influence of the road surface, smooth ice (VTI; 30 km h^{-1}).

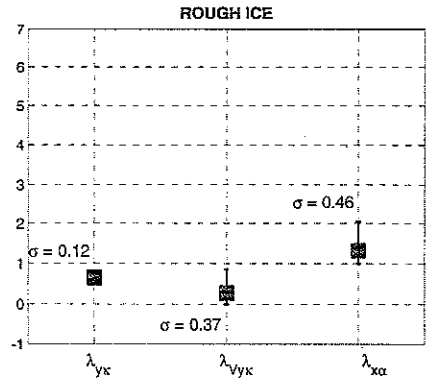

Figure 29. Combined-slip tests: influence of the road surface, rough ice (VTI; 30 km h^{-1}).

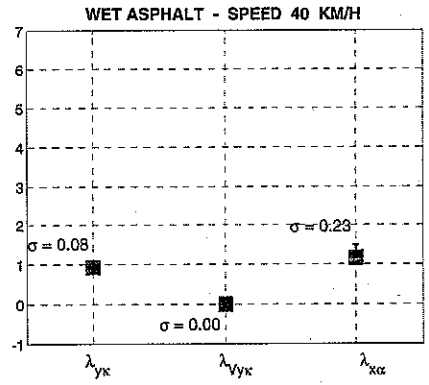

Figure 30. Combined-slip tests: influence of the test speed, 40 km h^{-1}, on wet asphalt.

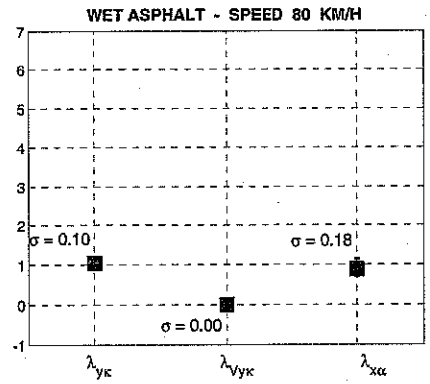

Figure 31. Combined-slip tests: influence of the test speed, 80 km h^{-1}, on wet asphalt.

Looking at figures 30 and 31 it can be seen that, even for combined-slip conditions, the speed of the test vehicle has almost no influence on the value of the scaling factors.

Because Nokian Tyres did not carry out a combined-slip test, the influence of the test vehicle cannot be investigated.

4. Conclusions

An extensive full-scale experimental test campaign was carried within the VERTEC European project (tasks 2a and 2b) to investigate, among other items, the influence of some overall important parameters, such as the road surface, test vehicle and weather conditions, on tyre behaviour. If the influence is interpreted in terms of MF tyre model using the scaling factors, the following conclusion can be drawn:

(1) The dispersion of scaling factor values is very small in most cases except for the shift scaling factors λ_{Hx}, λ_{Hy}, λ_{Vx}, and λ_{Vy} and the curvature scaling factor λ_{Ey} for pure lateral slip, owing to the lack of data at high slip angles.

(2) The influence of the road surface is mostly seen in the peak friction scale factors $\lambda_{\mu y}$ and $\lambda_{\mu x}$, as expected; also the stiffness scale factors λ_{Kx} and λ_{Ky}, are affected by surface roughness.
(3) The vehicle type does not influence the scaling factor values in pure longitudinal conditions; in pure lateral conditions, instead, λ_{Cy} and λ_{Ey} are affected by the vehicle type.
(4) The vehicle speed does not seem to influence scaling factor values.
(5) The dispersion of scaling factors in combined conditions is very small.

To validate the MF tyre model with identified scaling factor values a comparison between experimental data, collected on an instrumented passenger car, and MB simulations will be carried out in μ-split and μ-jump conditions.

Acknowledgements

We wish to acknowledge kindly the European Community for having funded this research project and all other partners, especially Mr Mancosu, coordinator of the VERTEC project (official contract G3RD-CT-2002-00805) and the partners involved in task 2a (*Reference tyre characterizations and tests*) and task 2b (*Development and validation of Tyre–Pavement interaction model*).

References

[1] Pacejka, H.B., 2002, *Tyre and Vehicle Dynamics* (Oxford: Butterworth-Heinemann).
[2] Pacejka, H.B. and Besselink, I.J., 1996, *MF-Tyre User Manual. A Design and Analysis Tool for Modelling and Simulation of Tyre Behaviour* (Delft: Delft Tyre).
[3] Nordström, O. and Åström, H., 2001, Upgrading of VTI friction test vehicle BV12 for combined braking and steering tests under aquaplaning and winter conditions. *Proceedings of the 2nd International Colloquium on Vehicle Tyre-Road Interaction*, Florence, Italy.
[4] Hakanen, J. and Kähärä, T., 2001, Tyre characterisation on ice and snow with a measurement vehicle. *Proceedings of the 2nd International Colloquium on Vehicle Tyre–Road Interaction*, Florence, Italy.
[5] Coleman, T.F. and Li, Y., 1996, An interior, trust region approach for non linear minimization subject to bounds. *SIAM Journal on Optimization*, **6**.

Vehicle System Dynamics
Vol. 43, Supplement, 2005, 475–482

Taylor & Francis
Taylor & Francis Group

Proposal of a tyre evaluation system with driving simulator under actual driving conditions

YOSHIHIRO SUDA*†, TAICHI SHIIBA§, YUSUKE TANABE‡ and MASAAKI ONUKI†

†Center for Collaborative Research,
‡Institute of Industrial Science, The University of Tokyo, 4-6-1 Komaba, Meguro-ku, Tokyo 153-8505, Japan
§Meiji University, 1-1-1 Higashimita, Tama-ku, Kawasaki-shi, Kanagawa-ken 214-8571, Japan

This article proposes a tyre evaluation system by using a driving simulator with a tyre testing machine. The dynamic characteristics of the tyre are important in the vehicle dynamics, hence the combination of tyre testing machine with driving simulator is examined to create virtual proving ground proposed by the authors. By applying measurement data from the tyre testing machine in real time instead of calculations by the tyre model, it is possible to get accurate tyre characteristics on a driving simulator. The actual prototype system was made and the dynamic tyre characteristics were evaluated. The experimental results were compared with the Magic Formula model and it was found that the proposed system has several features.

1. Introduction

The dynamic characteristics of a tyre are important in the vehicle dynamics. Tyre modeling is generally difficult and there is still room for research. For simulation purposes, tyre models like the Magic Formula are used in motion analysis of automobiles [1]. These are experimental models that describe the tyre characteristics, and cannot describe the dynamic characteristics. On the other hand, the detailed models which describe the dynamic characteristics or Finite-element method (FEM) models need many calculations, hence they are not suitable for motion analysis, which needs real time calculation like, driving simulator.

The authors' propose a 'virtual proving ground' which means a virtual running test environment with driving simulator [2]. In this article, by combining a tyre testing machine with a driving simulator, the virtual proving ground including the tyre and the tyre evaluation system by using driving simulator are proposed.

By applying measurement data from the tyre testing machine in real time instead of calculations by the tyre model, it is possible to get accurate tyre characteristics on a driving simulator.

*Corresponding author. Email: suda@iisu-tokyo.ac.jp

Vehicle System Dynamics
ISSN 0042-3114 print/ISSN 1744-5159 online © 2005 Taylor & Francis
http://www.tandf.co.uk/journals
DOI: 10.1080/00423110500246224

The test results of this system are compared with the experimental results produced using the Magic Formula model. Moreover, the double lane change test was conducted and compared for three types of tyres for vehicle dynamics on the driving simulator.

2. System and modelling

The system configuration proposed in this article is shown in figure 1. In the proposed system, the data of four tyres (the vertical force, the slip angle, and the slip ratio data of the tyre), which are calculated from dynamic calculation of the driving simulator are input into the tyre

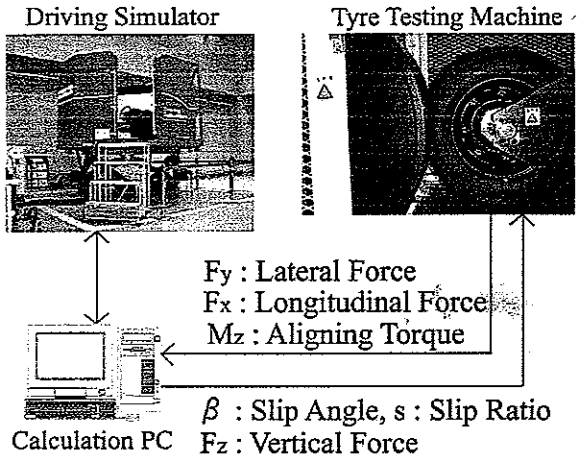

Figure 1. System configuration.

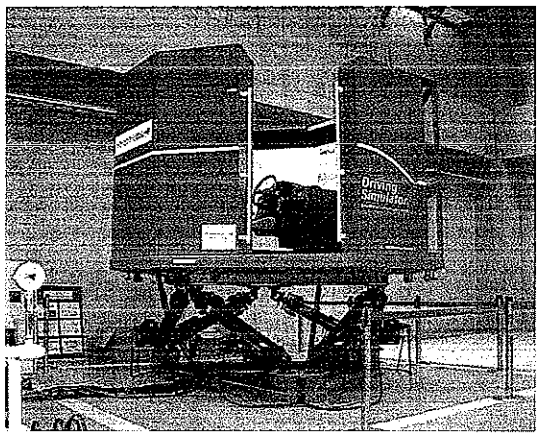

Figure 2. Driving simulator.

Table 1. Specification of automobile model.

Parameter	Value
Mass of body	1000 kg
Wheel base	2700 mm
Load distribution ratio	55:45 (front:rear)
Tread	1.5 m
Drive system	FF

testing machine. The lateral force, the longitudinal force, and the aligning torque are measured and measured data are used as input to calculate vehicle dynamics in real time. Presently, the tyre-testing machine does not have a braking and driving function. Therefore, in this article, the vertical force and the slip angle are input and the lateral force is used. In addition, only one tyre can be treated on the tyre testing machine. Therefore, the average vertical force and slip angle data of right and left front tyres are input and measured lateral force data are used as equal values for right and left front tyres. The longitudinal force of four tyres and the lateral force of rear tyres are calculated using the Magic Formula model.

The driving simulator used in this article is shown in figure 2. The automotive model is a small-sized passenger car with four wheels including rolling and pitching. The specifications of this model are shown in table 1.

3. Tyre characteristic test and model evaluation

Before performing the running test using this system, steady state characteristic test and dynamic characteristic test for three tyres used in this article were carried out. The tyre testing machine used in this article is shown in figure 3 and the specifications are shown in table 2. The specifications of the three tyres are shown in table 3. The basis tyre (tyre A), low profile tyre (that has nearly the same diameter and bigger rim size than tyre A), and sport tyre (that has same size as tyre A) are compared.

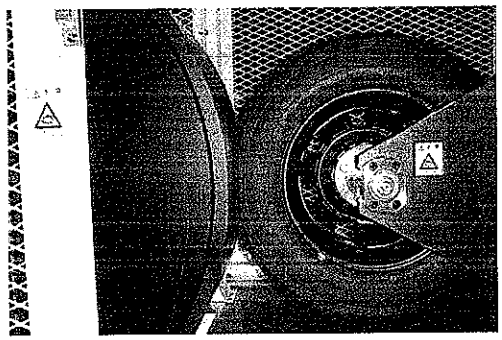

Figure 3. Tyre testing machine.